

NOTE TO USERS

This reproduction is the best copy available.

UMI^s

**EFFECT OF VALVE ELEMENT CHARACTERISTICS,
STRAY CAPACITANCE AND VOLTAGE HARMONICS ON
SURGE ARRESTER DIAGNOSTICS**

By

SUDATH NAMAL FERNANDO

A Thesis

Submitted to the Faculty of Graduate Studies

In Partial Fulfillment of the Requirements

For the Degree of

Master of Science

Department of Electrical and Computer Engineering
University of Manitoba,
Winnipeg, Manitoba

© Copyright by S. N. Fernando 2001



**National Library
of Canada**

**Acquisitions and
Bibliographic Services**

395 Wellington Street
Ottawa ON K1A 0N4
Canada

**Bibliothèque nationale
du Canada**

**Acquisitions et
services bibliographiques**

395, rue Wellington
Ottawa ON K1A 0N4
Canada

Your file Votre référence

Our file Notre référence

The author has granted a non-exclusive licence allowing the National Library of Canada to reproduce, loan, distribute or sell copies of this thesis in microform, paper or electronic formats.

The author retains ownership of the copyright in this thesis. Neither the thesis nor substantial extracts from it may be printed or otherwise reproduced without the author's permission.

L'auteur a accordé une licence non exclusive permettant à la Bibliothèque nationale du Canada de reproduire, prêter, distribuer ou vendre des copies de cette thèse sous la forme de microfiche/film, de reproduction sur papier ou sur format électronique.

L'auteur conserve la propriété du droit d'auteur qui protège cette thèse. Ni la thèse ni des extraits substantiels de celle-ci ne doivent être imprimés ou autrement reproduits sans son autorisation.

0-612-62725-X

Canada

**THE UNIVERSITY OF MANITOBA
FACULTY OF GRADUATE STUDIES

COPYRIGHT PERMISSION**

**EFFECT OF VALVE ELEMENT CHARACTERISTICS, STRAY
CAPACITANCE AND VOLTAGE HARMONICS ON SURGE
ARRESTER DIAGNOSTICS**

By

SUDATH NAMAL FERNANDO

**A Thesis/Practicum submitted to the Faculty of Graduate Studies of The University
of Manitoba in partial fulfillment of the requirement of the degree
of
Master of Science**

(c) 2001

**Permission has been granted to the Library of the University of Manitoba to lend or
sell copies of this thesis/practicum, to the National Library of Canada to microfilm
this thesis and to lend or sell copies of the film, and to University Microfilms Inc. to
publish an abstract of this thesis/practicum.**

**This reproduction or copy of this thesis has been made available by authority of the
copyright owner solely for the purpose of private study and research, and may only
be reproduced and copied as permitted by copyright laws or with express written
authorization from the copyright owner.**

Abstract

Metal Oxide Surge Arresters (MOSA) degrade in service under the influence of constant working voltage, internal partial discharges, non-uniform voltage distribution, possible moisture ingress and the occurrence of transient or sustained over-voltage; all of the above result in an increased value of resistive leakage current. The degradation of MOSA in service is diagnosed by using the third harmonic content of the resistive portion of the arrester leakage current as an indicator.

This thesis investigates errors in the diagnostic indicator due to the hysteresis character of the valve elements, the effect of stray capacitance and voltage harmonics.

A method is proposed to assess the discerning ability of the diagnostic indicator due to hysteresis character of the valve elements and voltage harmonics. Effect of stray capacitance on the diagnostic indicator is investigated by carrying out simulations in PSCADTM using a model developed in the present work.

The simulation results show that the diagnostic indicator is influenced by hysteresis character of the valve elements, stray capacitance and voltage harmonics. The diagnostic indicator is affected by the location of the aged valve element in the arrester column.

Acknowledgements

I would like to express my deep gratitude and appreciation to my thesis advisor, Dr. M.R. Raghuv eer, for suggesting the thesis topic, and for his constant guidance, encouragement and support.

The author is indebted to Prof. Rohan Lucas [University of Moratuwa, Sri Lanka] for his encouragement to do higher studies and arranging the opportunity to do so.

The author appreciate and acknowledge Mr. M. W. McDermit and Mr. Ahmad Glodjo [Manitoba Hydro] for their input to this work, Mr. John Kendall for his assistance in performing laboratory experiments, and Dr. Rohitha Jayasinghe [Manitoba HVDC Center] for valuable discussions on simulations using PSCAD/EMTDC.

Funding from Manitoba Hydro, the University of Manitoba, and the National Science and Engineering Research Council are gratefully acknowledged.

The author would also like to thank his colleagues for many stimulating discussions.

This acknowledgement would be incomplete without thanking the author's wife and parents for continuous support, understanding and encouragement in all aspects.

Table of Contents

| | |
|--|------|
| Abstract | iii |
| Acknowledgements | iv |
| Table of Contents | v |
| List of Tables | viii |
| List of Figures | x |
| List of Symbols | xii |
| | |
| CHAPTER 1 INTRODUCTION | 1 |
| 1.1 General Characteristic of Metal Oxide Valve Element | 1 |
| 1.2 Modeling of Metal Oxide Valve Element | 3 |
| 1.3 Deterioration of MOSA | 5 |
| 1.4 On-site Diagnostic Testing Techniques | 7 |
| 1.4.1 Measurement of total leakage current | 7 |
| 1.4.2 Direct measurement of the resistive leakage current | 8 |
| 1.4.3 Harmonic analysis of the leakage current | 8 |
| 1.4.4 Measurement of the temperature of MO valve element | 9 |
| 1.5 Scope of the Present Investigation | 9 |
| 1.5.1 Effect of hysteretic characteristics of the valve element on diagnostic indicator | 10 |
| 1.5.2 Off-center positioning of MO valve elements | 10 |
| 1.5.3 Simulation of 115 kV MOSA | 10 |
| | |
| CHAPTER 2 MODELING OF METAL OXIDE VALVE ELEMENTS | 12 |
| 2.1 Simple MO Valve Element Model | 13 |
| 2.2 Derivation of v-ir Characteristics of the Resistive Element. | 13 |
| 2.2.1 Experimental set-up to record voltage and leakage current | 14 |
| 2.2.2 Derivation of v-ir characteristics | 15 |
| 2.2.3 Derivation of simplified v-ir characteristics | 18 |

| | | |
|--|---|-----------|
| 2.3 | Capacitive Element of the MO Valve Element | 20 |
| 2.3.1 | Measurement of capacitance | 21 |
| 2.4 | The v-ir Characteristics of Off-Centered Valve Elements | 23 |
| CHAPTER 3 INFLUENCE OF HYSTERETIC V-IR CHARACTERISTICS ON DIAGNOSTICS | | 25 |
| 3.1 | Introduction | 25 |
| 3.2 | Evaluation of Discerning Ability of a Diagnostic Indicator | 26 |
| 3.2.1 | Evaluation procedure | 27 |
| 3.2.2 | Discussion | 29 |
| 3.3 | Investigation of Influence of Voltage Harmonics on the Diagnostic Indicator | 29 |
| CHAPTER 4 MODELING TECHNIQUE OF MO SURGE ARRESTER INCLUDING STRAY CAPACITANCE | | 34 |
| 4.1 | MOSA without Stray Capacitance | 34 |
| 4.2 | MOSA with Stray Capacitance | 35 |
| 4.3 | Aging of MO Valve Element | 42 |
| 4.4 | Simulation Procedure | 43 |
| CHAPTER 5 EFFECT OF STRAY CAPACITANCE AND AGEING ON MOSA DIAGNOSTIC INDICATOR | | 46 |
| 5.1 | Effect of Stray Capacitance on the Diagnostic Indicator | 46 |
| 5.2 | Effect of Ageing on the Diagnostic Indicator | 47 |
| 5.2.1 | Only one valve element pair is aged | 47 |
| 5.2.2 | Multiple valve elements are aged | 50 |
| 5.3 | Effect of Harmonics on the Diagnostic Indicator | 52 |
| 5.4 | Effect of Change in Capacitance of the VE due to Ageing | 53 |
| 5.5 | Practical Significance of Simulation Results | 54 |
| CHAPTER 6 CONCLUSIONS | | 55 |
| 6.1 | Summary | 55 |
| 6.2 | Conclusion | 56 |

| | |
|--|-----------|
| 6.3 Recommendations for Future Research | 56 |
| APPENDIX A INCLUSION OF COMPENSATION TECHNIQUE IN MANITOBA HYDRO TEST PROCEDURE | 57 |
| A.1 Laboratory Test Procedure | 57 |
| A.2 Voltage and Total Current Waveforms of the MOSA | 59 |
| A.3 The v-ir Characteristic of the MOSA | 59 |
| A.4 Application of Compensation Technique to Manitoba Hydro Test Procedure . | 61 |
| Reference List | 62 |

List of Tables

| | | |
|-----------|--|----|
| Table 2.1 | Results of experimental and simulation values of capacitance of MO valve element pair | 21 |
| Table 2.2 | Effect of off-centering on the diagnostic indicator (mA) of unaged arrester..... | 24 |
| Table 3.1 | Tabulation of current $I_{3r(NL+h)}$ and $I_{3r(NL)}$ at various voltages | 28 |
| Table 3.2 | Simulation results showing effect of voltage harmonics on the diagnostic indicator | 30 |
| Table 4.1 | Stray capacitances considered in the simulation | 35 |
| Table 4.2 | Voltage across the MO valve elements | 40 |
| Table 5.1 | Effect of stray capacitance on the diagnostic indicator (mA) of unaged arrester. Voltage harmonic content nil. Stray capacitance as per Table 4.1. VE capacitance constant. | 47 |
| Table 5.2 | Effect of ageing of VE #1 & #2 on the diagnostic indicator (mA). Voltage harmonic content nil. Stray capacitance as per Table 4.1. VE capacitance constant | 48 |
| Table 5.3 | Effect of ageing of VE #3 & #4 on the diagnostic indicator (mA). Voltage harmonic content nil. Stray capacitance as per Table 4.1. VE capacitance constant. | 48 |
| Table 5.4 | Effect of ageing of VE #5 & #6 on the diagnostic indicator (mA). Voltage harmonic content nil. Stray capacitance as per Table 4.1. VE capacitance constant | 48 |
| Table 5.5 | Effect of ageing of VE #7 & #8 on the diagnostic indicator (mA). Voltage harmonic content nil. Stray capacitance as per Table 4.1. VE capacitance constant | 49 |
| Table 5.6 | Effect of ageing of VE #9 & #10 on the diagnostic indicator (mA). Voltage harmonic content nil. Stray capacitance as per Table 4.1. VE capacitance constant | 49 |
| Table 5.7 | Effect of ageing of four VE's on the diagnostic indicator (mA). Voltage harmonic content nil. Stray capacitance as per Table 4.1. VE capacitance constant | 50 |

| | | |
|-----------|--|----|
| Table 5.8 | Effect of voltage harmonics on the diagnostic indicator (mA). Distributed stray capacitance as per DS2 (Table 4.1). VE capacitance constant. | 52 |
| Table 5.9 | Effect of change in the capacitance on the diagnostic indicator (mA). Voltage harmonic content nil. Stray capacitance as per Table 4.1. | 53 |

List of Figures

| | | |
|----------|---|----|
| Fig. 1.1 | a) Microstructure and construction of ZnO valve element b) Schematic representation of series and parallel arrangement of grains and junctions. A:Connections; B:Metallic electrodes; C:Intergranular layers; D:ZnO grains [2]. | 2 |
| Fig. 1.2 | Typical voltage-current characteristics of a metal oxide disc (80 mm diameter, 20 mm height) [3] | 3 |
| Fig. 1.3 | Representation of metal oxide valve element. | 4 |
| Fig. 2.1 | Simplified representation of MO valve element | 12 |
| Fig. 2.2 | Schematic diagram of single phase laboratory set-up to obtain applied voltage and leakage current. [V.E.: MO valve element] | 13 |
| Fig. 2.3 | Applied voltage and leakage current waveforms for unaged MO valve element pair | 14 |
| Fig. 2.4 | Waveform of applied voltage, capacitive current and resistive current of MO valve element pair. | 16 |
| Fig. 2.5 | v-ir characteristic curve of MO valve element pair at voltage of 11.5 kV. | 17 |
| Fig. 2.6 | v-ir characteristics at different voltages [10.5 kV, 11.0 kV, 11.5 kV]. | 18 |
| Fig. 2.7 | Simplified v-ir curve for unaged MO valve element pair | 19 |
| Fig. 2.8 | Experimental and simulation values of capacitance for unaged and aged MO valve elements | 23 |
| Fig. 3.1 | v-ir characteristics of MO valve element | 27 |
| Fig. 3.2 | Applied voltage. Continuous curve is contaminated with harmonics and the other is pure sine wave | 31 |
| Fig. 3.3 | Resistive current corresponding to harmonic contaminated voltage (thin continuous line) and pure sine voltage | 32 |
| Fig. 4.1 | MOSA without strays | 35 |
| Fig. 4.2 | MOSA with strays | 36 |
| Fig. 4.3 | Algorithm used in calculating resistive element R | 38 |
| Fig. 4.4 | PSCAD case | 39 |

| | | |
|----------|---|----|
| Fig. 4.5 | Voltage distribution along the MOSA. 1.0 p.u. corresponds to uniform voltage distribution i.e. 9.429 kV rms. | 42 |
| Fig. 4.6 | Simplified v-ir characteristics for unaged and aged MO valve element pair | 43 |
| Fig. 4.7 | Waveforms of arrester voltage and total arrester current from simulated results. | 44 |
| Fig. 4.8 | Waveform of applied voltage, arrester capacitive and resistive currents. . | 45 |
| Fig. A.1 | Test Data sheet for a 33 kV arrester [Courtesy Manitoba Hydro] | 58 |
| Fig. A.2 | Applied voltage and total leakage current. | 60 |
| Fig. A.3 | Waveform of applied voltage, capacitive current and resistive current of MOSA. | 60 |
| Fig. A.4 | v-ir characteristics curve of MOSA | 61 |

List of Symbols

| | |
|----------------|---|
| C | Capacitance of metal oxide valve element |
| I_c | Capacitive leakage current of MOSA |
| I_R, i_r | Resistive leakage current of MOSA |
| I_t | Total leakage current of MOSA |
| $I_{3r(NL+h)}$ | 3rd harmonic content of the resistive component |
| $I_{3r(NL)}$ | 3rd harmonic content of the resistive component when applied voltage is a pure sinusoid |
| L | Inductance of metal oxide disk |
| R | Non-linear capacitance of metal oxide valve element |
| R_i | Resistance of the granular layer |
| R_z | Resistance of ZnO grains |
| V, v | Voltage across the arrester |
| C_{gn0} | Stray capacitance from valve element to ground |
| ρ | Resistivity in Ωm |

CHAPTER 1 Introduction

The primary function of a Metal Oxide Surge Arrester (MOSA) is to protect transmission and distribution equipment from overvoltages and to absorb electrical energy resulting from lightning or switching surges and from temporary overvoltages [1]. The active part of the arrester consists of series-connected metal oxide valve elements.

1.1 General Characteristic of Metal Oxide Valve Element

Metal Oxide (MO) valve elements are ceramic resistors with a highly nonlinear current-voltage characteristic applicable for transient overvoltage suppression. The nonlinear resistivity is an inherent bulk property of this composite ceramic resistor, which consists mainly of ZnO with a relatively small amount of several additives of other metal oxides such as Bi_2O_3 , CoO , MnO_3 , Sb_2O_3 . These additives determine essentially the electric properties of the valve element. On a macroscopic scale the additives are almost homogeneously distributed throughout the varistor body. The microstructure of the composite ceramic is built up of electrically conducting ZnO grains separated by grain boundaries or

thin intergranular phases of significantly different composition. The varistor therefore represents a network of series and parallel arrangements of highly doped ZnO grains separated by intergranular junctions. These junctions contain localized charges which give rise to depletion regions within the doped grains and, as a consequence, to symmetrical Schottky barriers at the grain boundaries. These barriers cause the observed nonlinear conduction [2]. Fig. 1.1(a) shows the microstructure of a metal oxide valve element and Fig. 1.2(b) its schematic representation. For a large number of grains in parallel and series the two structures lead, statistically, to the same electric properties.

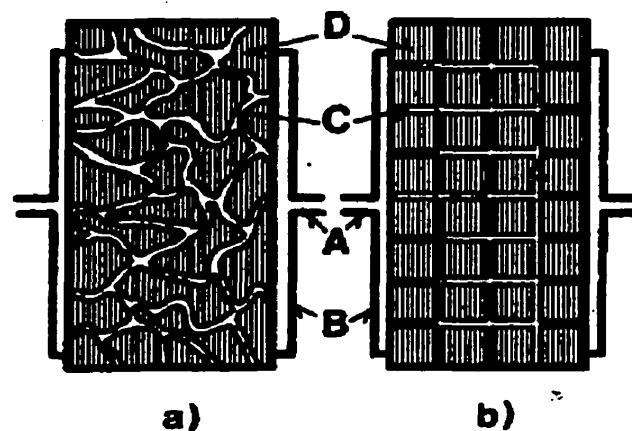


Fig. 1.1 a) Microstructure and construction of ZnO valve element b) Schematic representation of series and parallel arrangement of grains and junctions.
A:Connections; B:Metallic electrodes; C:Intergranular layers; D:ZnO grains [2]

The nominal voltage of a valve element is proportional to its length. The valve elements of equal cross section can be connected in series (stacking), whereby the nominal voltages are added. The current carrying capacity of a valve element is proportional to its cross section.

1.2 Modeling of Metal Oxide Valve Element

The experimentally derived voltage-current characteristics of a standard metal oxide valve element, 80 mm in diameter and 20 mm high, is shown in Fig. 1.2 for different temperatures [3]. The variation of the resistive component I_r and the capacitive component I_c of the current through the metal oxide disk may be explained on the basis of the conduction mechanism of the microstructure shown in Fig.1.1.

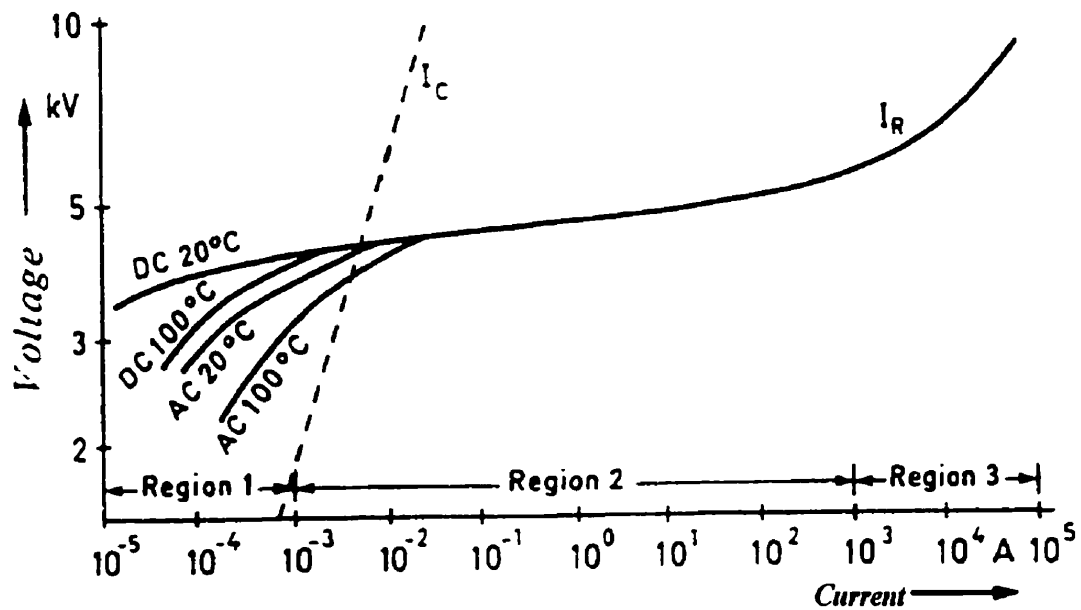


Fig. 1.2 Typical voltage-current characteristics of a metal oxide disc (80 mm diameter, 20 mm height) [3]

As seen from Fig. 1.2, the characteristics of the resistive component are divided into three regions. The conduction mechanism in the region 1 is explained by means of energy barriers in the granular layer. The barrier prevents electrons from moving from one layer to

another. An electric field has the effect of lowering these barriers and electrons pass over them thermally. This is called Schottky emission and gives rise to small current through the material.

In the middle and high electric field regions, the conduction mechanism of metal oxide valve element can be explained by the tunnel effect and reversed-biased Schottky emission respectively [3].

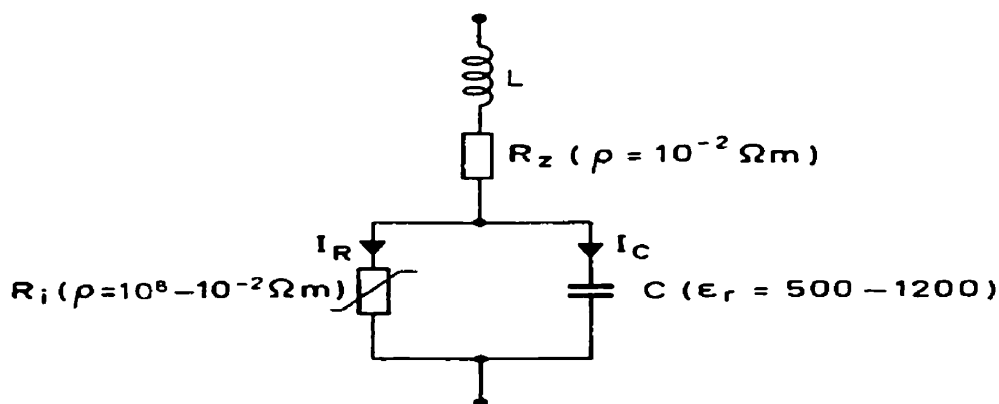


Fig. 1.3 Representation of metal oxide valve element.

For the entire operating region a valve element may be represented as in Fig 1.3 [3]. Here, R_i represents the non-linear resistance of the granular layers, where the resistivity ρ changes from $10^8 \Omega m$ for low electric field stress to just below $0.01 \Omega m$ for high stress. The granular layer has a relative dielectric constant between 500 to 1200 depending on the

manufacturing process; R_z is the resistance of the ZnO grains with resistivity of about $0.01 \Omega\text{m}$; L represents the inductance of the metal oxide disc and is determined by the geometry of the current flow path.

The objective of arrester application is to select the lowest rated surge arrester that will have a satisfactory service life on the power system while providing adequate protection of equipment insulation. An arrester of the minimum practical voltage rating is generally preferred because it provides the greatest margin of protection for the insulation. The use of a higher voltage rating increases the capability of the arrester to survive on the power system, but reduces the margin of protection it provides for a specific insulation level. Thus, arrester selection must strike a balance between arrester survival and equipment protection. The continuous operating voltage of an arrester falls within region 1. The scope of this thesis is limited to a study of arrester characteristics in region 1 as shown in Fig. 1.2.

In region 1, $R_z \ll R_i$ and inductance L can be neglected. Therefore in the normal operating region we can model the metal oxide valve element as a nonlinear resistor with linear capacitive element in parallel. Characteristics of the non-linear resistor and capacitive valve element are discussed in Chapter 2.

1.3 Deterioration of MOSA

MOSA degrades in service under the influence of constant working voltage, internal partial discharges, non-uniform voltage distribution, possible moisture ingress and the occur-

rence of transient or sustained over-voltage; all of the above result in an increased value of resistive leakage current [4].

Internal partial discharges cause degradation of MOSA. It is known that some gases may be formed in service because of partial discharge inside the MOSA housing. The granular layer of MOSA reacts chemically with the surrounding unstable gas molecules, which results in the deterioration of the electrical property of the combination of ZnO and its granular layers. To limit this effect, measures may be taken in the process of selection of MOSA and sealing techniques.

The axial voltage distribution is affected by the stray capacitance. The existence of any stray capacitance will cause a non-uniform voltage distribution. Thus, the gradient will be higher than the average across the valve element near the top, and lower than the average across valve elements near the bottom. If the axial voltage is non-uniform, premature ageing of some valve elements will result in the short lifetime of the arrester [5].

A high transient or sustained voltage, hence a high current stress on MOSA, will also cause the degradation in MOSA. High current through MOSA results in an excessive local current density through the granular layers, and this may partially destroy them.

Thus, with the passage with time, a MOSA may exhibit ageing. The aged MOSA manifests itself in an increased component of resistive leakage current, especially the 3rd harmonic component. A serious consequence of this increased leakage current is that the energy absorption capability decreases which in turn may lead to thermal runaway and

cause failure of MOSA. Therefore, it is very important to periodically check the condition of MOSA in service to ensure that its operating characteristics are acceptable.

1.4 On-site Diagnostic Testing Techniques

Different methods have been proposed for monitoring the condition of MOSA. Some of these techniques are based on the measurement of radio interference, partial discharge and emitted electromagnetic radiation. However, these methods may not detect the real operating condition of MOSA due to interference from the other sources on-site.

On the other hand, diagnostic techniques based directly on the measurement of leakage currents are popular and have offered the most promise. These methods which are currently used for on-site diagnostics include: measurement of the total current [6], the resistive leakage current [7, 8], higher order harmonic currents in the total current [1] and the zero sequence current measuring method [9].

As an alternative to leakage based methods, the temperature of MO valve element can be used for diagnosis purposes [10].

1.4.1 Measurement of total leakage current

Measurement of the total leakage current is commonly implemented by means of a permanently installed milliampere-meter, which shows the average of the rectified leakage current, or by a portable instrument for average and peak level measurements. These measurements have a very low sensitivity and are inadequate for determining the condition of MOSA [12].

1.4.2 Direct measurement of the resistive leakage current

A direct determination of the resistive leakage current component is the most desirable method since it allows an immediate comparison with the expected level of resistive current at the prevailing operating condition. The resistive component of the current is found by registering the leakage current at the instant when the voltage across the arrester is at its peak. However, this method is usually hard to apply in practice. First, it requires that the voltage across the arrester be measured simultaneously with the leakage current and, secondly, the phase shift of the voltage measurement to be negligible. Furthermore, it is required that potential transformers fulfilling this requirement, are present in all phases, and that the connections can be made during the operation of the system.

It is very difficult to satisfy all the conditions for in-service diagnosis. Therefore direct measurement of the resistive leakage current is possible to perform only in special cases. This method could be used in a laboratory setup. Manitoba Hydro uses such a method to check the condition of MOSA in a laboratory setup as well as under field conditions. The method used by Manitoba Hydro is discussed briefly in Appendix A.

1.4.3 Harmonic analysis of the leakage current

Due to the non-linear resistance of the metal oxide valve element, the leakage current contains harmonics when the arrester is energized with a sinusoidal voltage. Since the amplitude of the harmonic currents increase with the resistive component of the leakage current, the harmonic content can be used as an indicator of the arrester condition.

Different implementations of this method have been presented in the past: Determination of the ratio of the sum of the harmonics to the total leakage current [11], and measurements of the third order harmonic current alone [1]. The presence of harmonics in the system may, however, interfere with the harmonics generated by the non-linear resistance of the surge arrester. To compensate for this error a new method was proposed in [12]. A diagnostic instrument based on [12] is available at Manitoba Hydro. This instrument uses a field probe to compensate for harmonics in the system voltage. The diagnostic indicator is influenced by the probe position [4] and this may again lead to errors.

1.4.4 Measurement of the temperature of MO valve element

There are several parameters that effect the temperature of the MO column. At any time, independent of element history, the energy absorption capability of the arrester is determined by the actual MO valve element temperature [10]. Therefore, the temperature of the MO column can be used as a criterion whether the arrester is working in (thermally) stable condition or not. The recent development of a temperature measurement technique which allows remote measurement of temperature by passive sensors directly within the MO column [13], gives rise to the possibility of using temperature as a diagnostic indicator.

1.5 Scope of the Present Investigation

In this study the 3rd harmonic component of the resistive current is considered as the diagnostic indicator. This thesis investigates errors in the diagnostic indicator due to the hysteresis character of the valve elements, the effect of stray capacitance from a tall arrester

column, valve element non-homogeneity and off center positioning of the valve elements (porcelain housing).

1.5.1 Effect of hysteretic characteristics of the valve element on diagnostic indicator

The third harmonic content consists of two components, i.e., a component due to the non-linear volt-ampere characteristics of the MOSA and an error component due to the presence of voltage harmonics. In previous work [14] the discerning ability of a diagnostic method to the error component was investigated using simplified $v-i_r$ characteristics. In the present study a similar analysis is carried out considering the hysteretic nature of the valve element. The proposed method involves the experimental determination of the $v-i_r$ characteristics of an arrester followed by a simulation procedure which calculates the third harmonic currents. This aspect is discussed in detail in Chapter 3.

1.5.2 Off-center positioning of MO valve elements

In the older versions of porcelain type MOSA, there is a gap between the arrester stack and the porcelain case. Due to this gap and due to handling valve elements may not be lined up vertically. The effect of this off-centering on the diagnostic indicator is investigated. Results are given in Chapter 2.

1.5.3 Simulation of 115 kV MOSA

A 115 kV arrester was simulated using PSCAD/EMTDC[†]. This allows the investigation of stray capacitance effects and ageing of individual valve elements. Chapter 4 deals with

modeling of MOSA with stray effects and the simulated results for various cases are given in Chapter 5.

† EMTDC is a general purpose time domain simulation program for simulating power systems transients and its controls. PSCAD is its integrated graphical user interface.

CHAPTER 2 Modeling of Metal Oxide Valve Elements

As indicated in Chapter 1, a Metal Oxide (MO) valve element can be modelled as a non-linear resistor in parallel with a capacitive element. Fig. 2.1 shows the simple model considered in this thesis. This chapter deals with finding the characteristics of the resistive element and the value for the capacitive element.

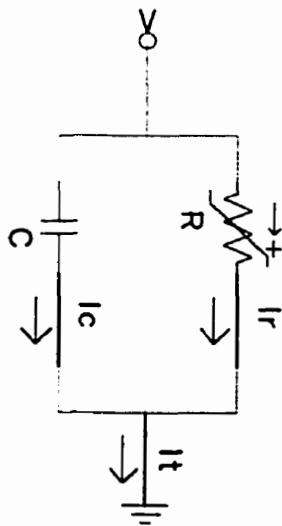


Fig. 2.1 Simplified representation of MO valve element

2.1 Simple MO Valve Element Model

Under normal operating conditions, there is a small leakage current, I_r , in the arrester. This current contains two components: a resistive component, I_r , due to the resistive element and a capacitive component, I_c , due to the capacitive element. The resistive component of the current through the MO valve element depends on the granular layer and is thus influenced by the manufacturing process, selection of the material and production. Hence, a considerable variation of the resistive current characteristics for different production lots and, in particular, for different manufacturers should be expected [3]. Typically I_r is in the range of 50 to 250 μA [12].

2.2 Derivation of v - i_r Characteristics of the Resistive Element.

The derivation of v - i_r characteristic requires experimental data and use of a software program to implement a numerical technique. The experimental set-up is shown in Fig. 2.2.

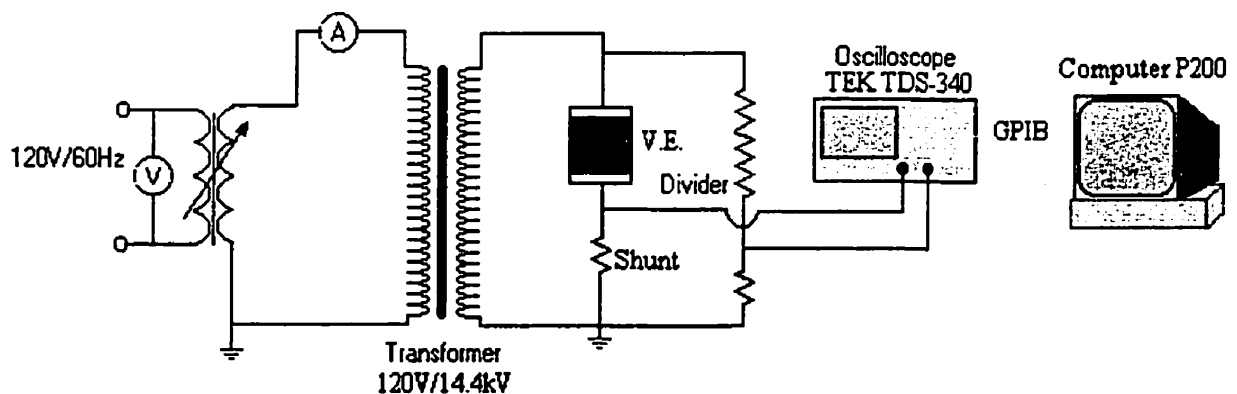


Fig. 2.2 Schematic diagram of single phase laboratory set-up to obtain applied voltage and leakage current. [V.E.: MO valve element]

2.2.1 Experimental set-up to record voltage and leakage current

The laboratory set-up is shown in Fig. 2.2.; two MO valve elements were used in series. The dimensions of the disk were 40 mm in height and 35 mm in diameter. The shunt is purely resistive with resistance value of 9.94 k Ω . The resistive divider ratio is 1000:1 [100M Ω / 10k Ω]. The total current through the valve element was measured by measuring the voltage across the shunt and total applied voltage was obtained through the divider. These two signals were captured using digital storage oscilloscope TEK 340 [15].

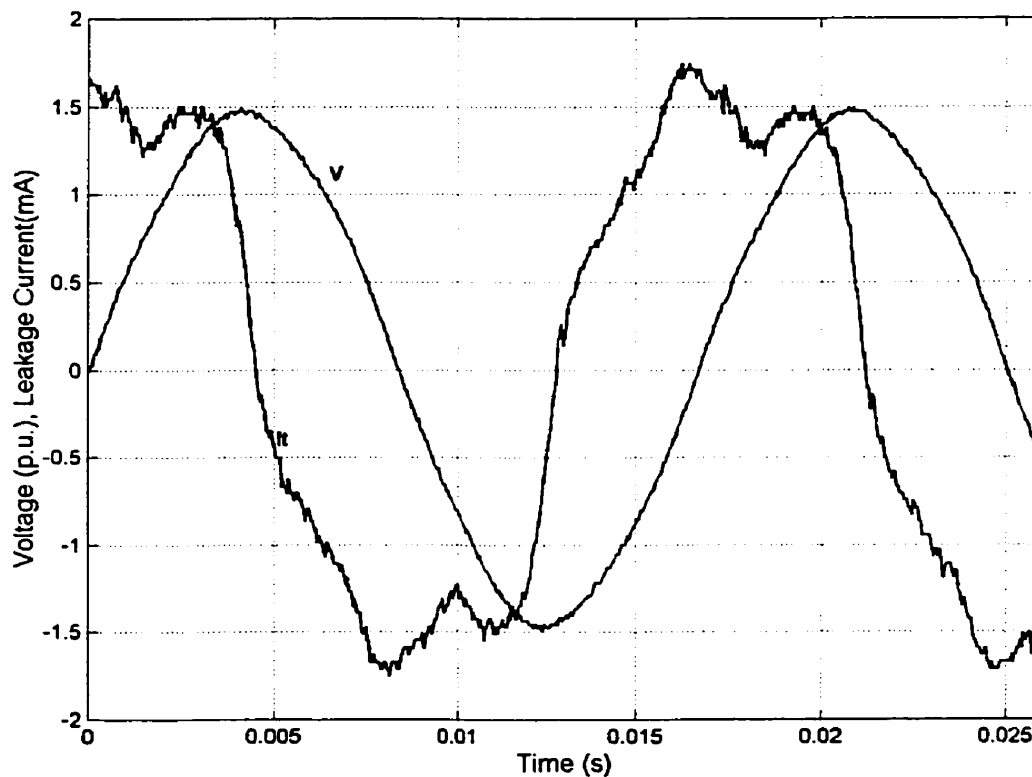


Fig. 2.3 Applied voltage and leakage current waveforms for unaged MO valve element pair.

Fig. 2.3 shows voltage and current waveforms obtained for an applied voltage of 11.5 kV for a unaged[†] MO valve element pair. Voltages are expressed in p.u. using a base of 11 kV for the valve element pair.

Once the voltage and total current had been obtained, the resistive leakage current was found by using a technique described in the following section.

2.2.2 Derivation of v - i_r characteristics

Using the Compensation Technique described in [4] the v - i_r characteristic for the MO valve element can be found. This characteristic essentially describes the nonlinear behavior of the resistive element.

The Compensation Technique is a numerical method which employs the orthogonal property of I_r and I_c to calculate the value of capacitance, C [Fig. 2.1 on page 12]. A detailed discussion on the capacitive element is included in section 2.3. Once the capacitance and fundamental and harmonic components of the applied voltage are known, I_c due to fundamental voltage and other harmonics present in the applied voltage can be calculated. Since the voltage magnitude of the harmonics above the 11th order are usually small, I_c due to these voltages are neglected. Knowing I_c , I_r can be found by removing the capacitive component from the total current. Fig. 2.4 shows the voltage, capacitive current and resistive current corresponding to the waveforms shown in Fig. 2.3.

[†] Previous work by Zhu [4] categorized valve elements into unaged, aged and damaged based on their simplified v - i_r characteristics.

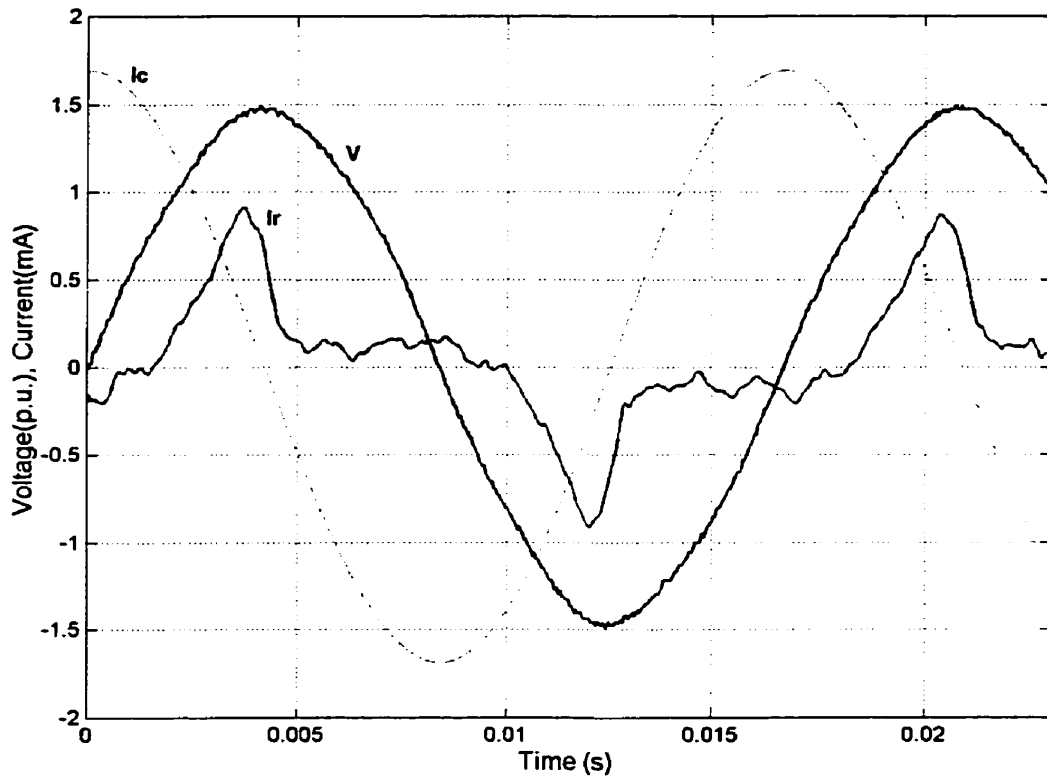


Fig. 2.4 Waveform of applied voltage, capacitive current and resistive current of MO valve element pair.

It has to be noted that I_r is not symmetrical about its peak value. This unsymmetrical nature can be clearly seen in Fig. 2.5 which shows the $v-i_r$ characteristic of the resistive element. There is a zero offset in I_r and it is high compared to Manitoba Hydro's measured data. In Manitoba Hydro, they use a technique based on hardware implementation where as in this work software based method, which does not account for any inductance in the circuit, is used.

This characteristic is unique to the resistive element for the particular peak value of the applied voltage used to derive it (i.e. 11.5 kV) and it is independent of the harmonic content in the applied voltage. This characteristic shows a hysteretic behavior, and an explanation of this behavior is beyond the scope of this thesis.

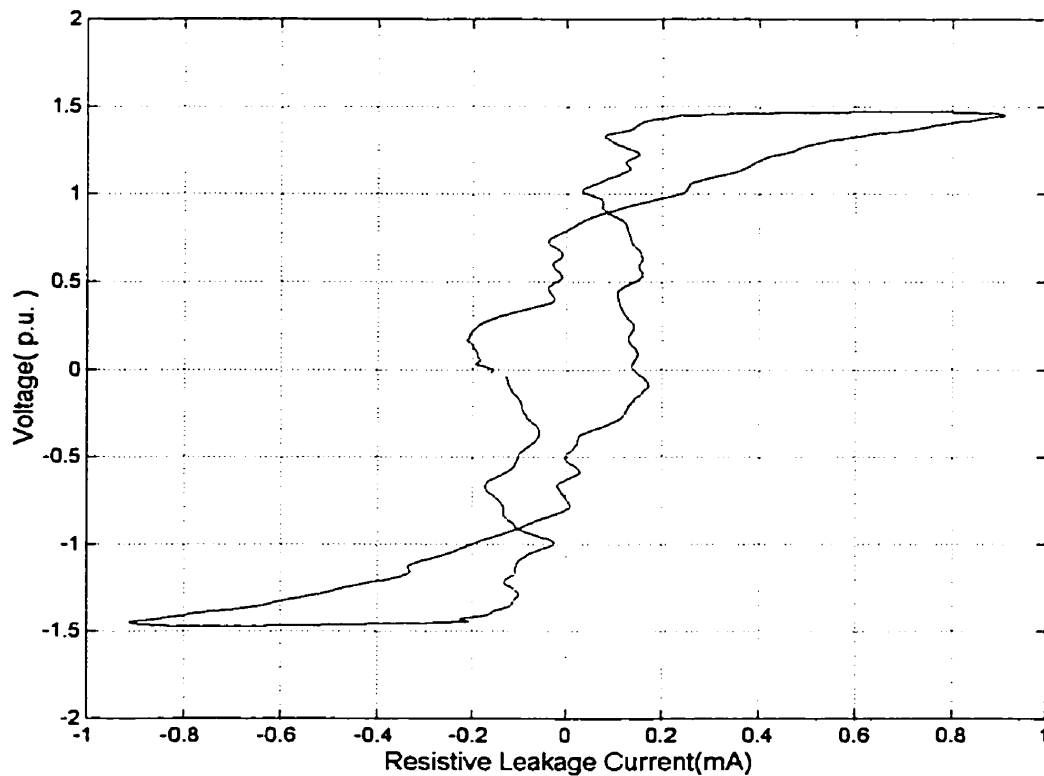


Fig. 2.5 $v-i_r$ characteristic curve of MO valve element pair at voltage of 11.5 kV.

The $v-i_r$ characteristics for different voltages were obtained and Fig. 2.6 shows a few such curves that have been used to find the simplified $v-i_r$ curve of the MO valve element as described in the next section.

The $v-i_r$ characteristics of an actual arrester tested by Manitoba Hydro is shown in Fig. A.4 of Appendix A. This characteristic was derived using Manitoba Hydro's experimental data [Fig. A.1 on page 58] and the Compensation Technique. In Appendix A the possibility of including the Compensation Technique in Manitoba Hydro's test procedure is suggested.

The $v-i_r$ characteristic is sensitive to temperature of the MO valve elements. Therefore when collecting data, a sufficient time interval should be allowed between two successive readings so that data is not effected by the temperature rise in the MO valve element.

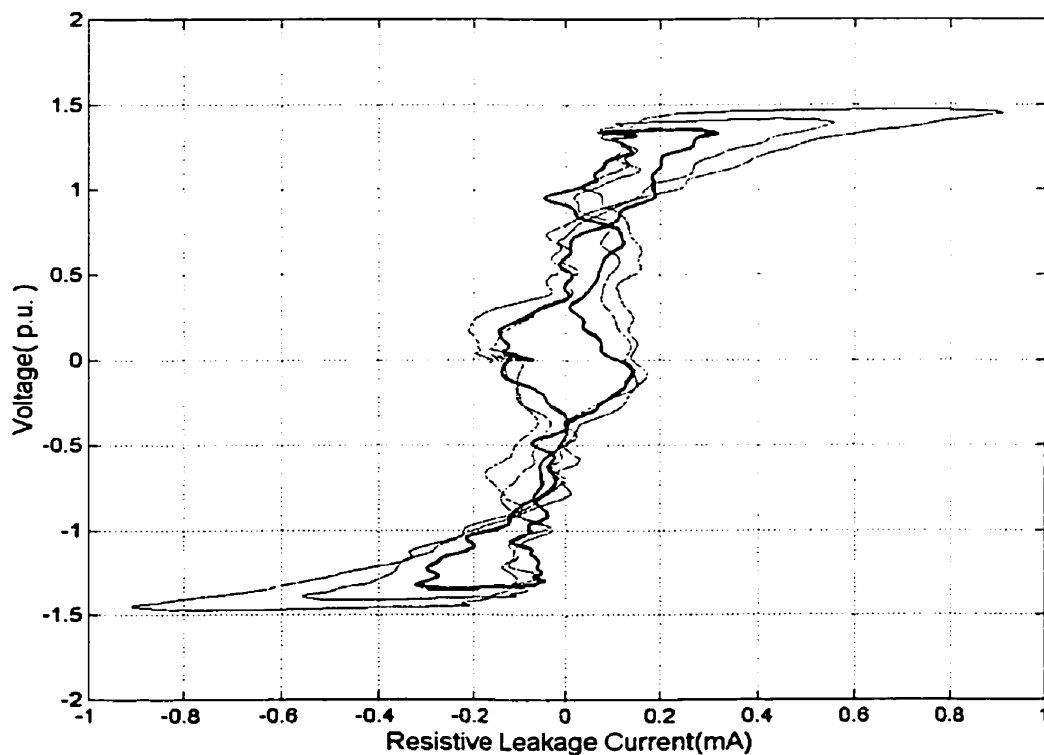


Fig. 2.6 $v-i_r$ characteristics at different voltages [10.5 kV, 11.0 kV, 11.5 kV].

2.2.3 Derivation of simplified $v-i_r$ characteristics

Surge arresters consist of several valve elements in series to obtain a desired protection level. To model a surge arrester, we need the $v-i_r$ characteristics for the valve element which are valid for the range of voltages considered in the simulation. Accurate modeling requires either analytical or experimental determination of the $v-i_r$ relation for voltages considered in the simulation. An analytical approach is very difficult if not impossible. Experimental determination is not practical since it requires determination of the $v-i_r$ characteristics at many voltages covering the expected range of voltage variations in practice.

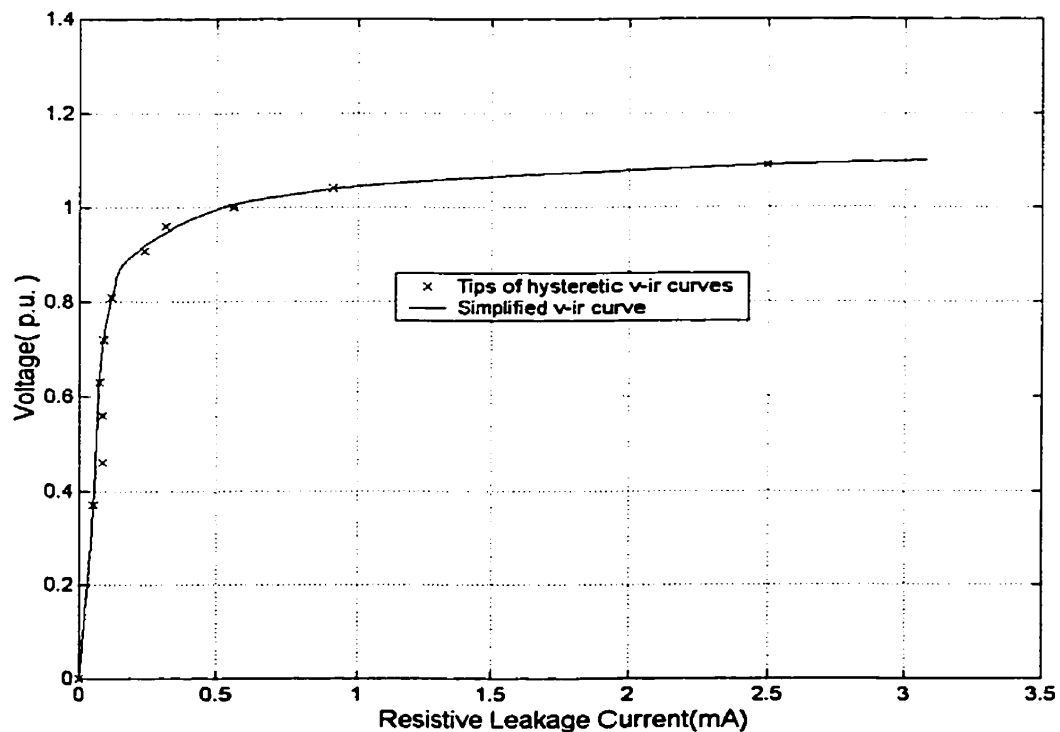


Fig. 2.7 Simplified $v-i_r$ curve for unaged MO valve element pair. [1.0 p.u. = 15.56 kV]

To overcome this problem, a simplified $v-i_r$ characteristic, which approximates the resistance of the MO valve element was derived. This curve is the locus of the tips of the $v-i_r$ characteristics obtained using the laboratory set-up [Fig. 2.2 on page 13].

Fig. 2.7 shows the experimental data corresponding to the tips of the $v-i_r$ characteristics and the simplified $v-i_r$ characteristics of an unaged MO valve element pair. The simplified curve is a multi-segment polynomial representation. From examination of the data in Fig. 2.7, it is obvious that the $v-i_r$ relationship is prominently nonlinear for $v > 0.81$ p.u. For $v \leq 0.81$ p.u the nonlinearity, although evident, is not as pronounced. A two segment polynomial representation is therefore proposed. It was found that a good fit could be achieved by using a fifth order polynomial representation. In the voltage range $v \leq 0.81$ p.u, the polynomial representation is given by:

$$i_r = 0.5294v^5 - 0.5453v^3 + 0.1619v^2 + 0.1492v \quad (2. 1)$$

and for the voltages greater than 0.81 p.u., the representation is:

$$i_r = [0.9579v^5 - 4.3384v^4 + 7.8505v^3 - 7.0932v^2 + 3.1997v - 0.5764] \times 10^4 \quad (2. 2)$$

However these equations can not be directly used in the simulation model discussed in Chapter 4. In the simulation model nonlinear resistance is represented in the form of a data file that agrees with $v-i_r$ characteristic. Therefore a data file is created to represent the derived equation and in the data file, the step length of voltage is 0.01 p.u. If voltage and resistive current are known, the nonlinear resistance of the valve element is the ratio between instantaneous voltage and current. In the simulation model a data file represent-

ing voltage and resistance is used. Simplified $v-i_r$ characteristic for an aged element set was also obtained and handled in a similar manner.

2.3 Capacitive Element of the MO Valve Element

The capacitance of the MO valve element depends only weakly on the applied voltage, temperature and frequency [16]. Temperature dependency is not considered in this thesis. This section deals with voltage dependency of the capacitive element. The physics behind the voltage-current properties are discussed in [17].

The typical specific capacitance of the MO valve element is 75 pF.kV/cm^2 and typical values of the capacitive current range from 0.5 to 3 mA [12]. For a complete surge arrester, the capacitive current depends on the number of valve elements in parallel, the stray capacitance and the actual operating voltage.

2.3.1 Measurement of capacitance

The capacitance of a MO valve element pair for different voltages were measured using the Capacitive and Tan Delta Bridge [18]. The results for unaged and aged valve elements are given in Table 2.1.

Table 2.1 Results of experimental and simulation values of capacitance of MO valve element pair. Capacitance is given in pF.

| Voltage [kV] | Unaged | | Aged | |
|-----------------|--------------|------------|--------------|------------|
| | Experimental | Simulation | Experimental | Simulation |
| 1.0 | 296.33 | | 328.31 | |
| 2.0 | 295.76 | | 326.28 | |
| 3.0 | 293.68 | | 322.28 | |

Table 2.1 Results of experimental and simulation values of capacitance of MO valve element pair. Capacitance is given in pF.

| Voltage [kV] | Unaged | | Aged | |
|-----------------|--------------|------------|--------------|------------|
| | Experimental | Simulation | Experimental | Simulation |
| 4.0 | 290.48 | 282.86 | 315.62 | 320.96 |
| 5.0 | 286.56 | 284.07 | 308.88 | 315.90 |
| 6.0 | 281.55 | 278.04 | 302.73 | 310.11 |
| 7.0 | 276.71 | 278.28 | 296.93 | 300.47 |
| 8.0 | 271.97 | 273.70 | 292.63 | 297.57 |
| 9.0 | | 272.49 | | 293.95 |
| 10.0 | | 268.87 | | 295.40 |
| 11.0 | | 278.50 | | 299.50 |

Measurements were made up to 8.0 kV rms. The capacitance found using the Compensation Technique is also tabulated. At very low voltages the resistive current is so insignificant that the Compensation Technique can not be used to calculate capacitance accurately.

The capacitance values derived from experiment and simulation are close and the trend of variation is similar for aged and unaged MO valve elements. Both techniques, experimental and simulation, assume MO valve elements to be modelled as a nonlinear resistor in parallel with a capacitive element [Fig. 2.1 on page 12]. The capacitance of the MO valve element depends on the voltage; thus the value found in both methods yield only the average value of valve element capacitance. For a more accurate value, mixed voltage tests [19] where the ratio of the AC component to the total voltage can be varied, may be used. In this method a very small alternating voltage is superimposed on a larger direct voltage. The alternating voltage level is then kept constant and direct voltage is varied. The capacitance of the MO valve element is measured using special setups and bridges.

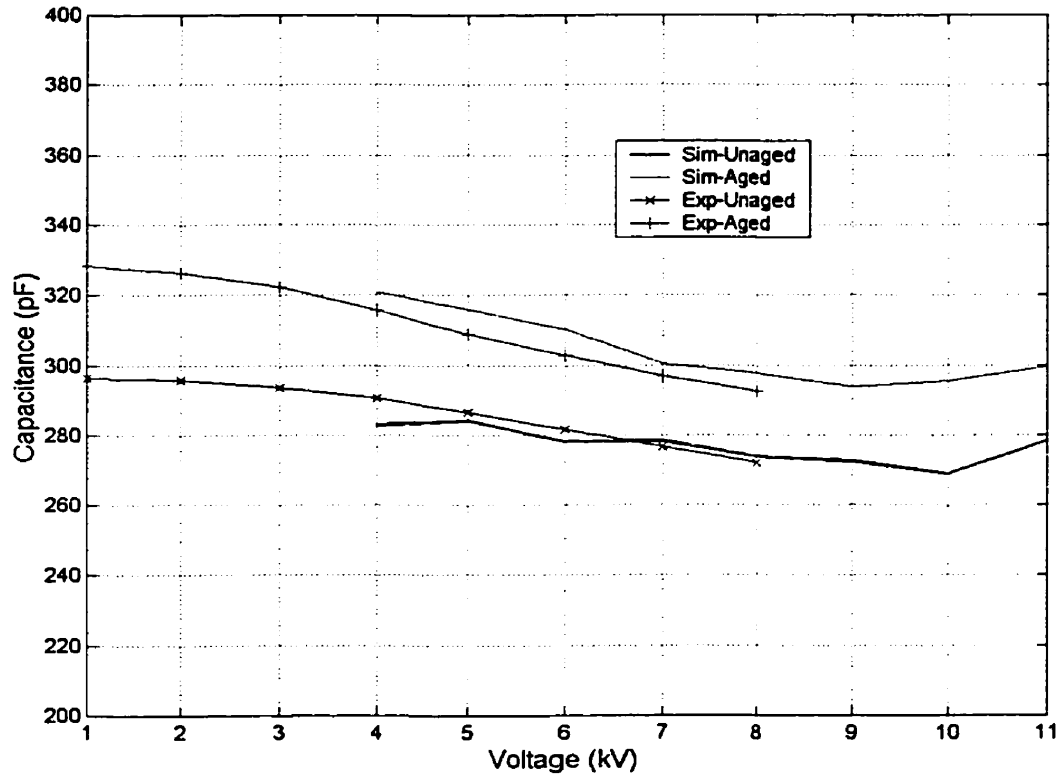


Fig. 2.8 Experimental and simulation values of capacitance for unaged and aged MO valve elements

2.4 The $v-i_r$ Characteristics of Off-Centered Valve Elements

Due to the air gap between MO valve elements and its casing, in a porcelain housing, MO valve elements may be off-centered. Effect of this was examined using the set-up shown in Fig. 2.2. Due to off-centering, the contact surface between two adjacent MO valve elements are reduced. Three cases were considered.

1. There is no off-centering i.e. 100% of the surfaces are in contact.
2. Only 95% of the surfaces are in contact due to off-centering
3. Only 90% of the surfaces are in contact due to off-centering

The magnitude of diagnostic indicator (obtained experimentally) for different cases with varying voltages are shown in Table 2.2.

Table 2.2 Effect of off-centering on the diagnostic indicator (μA) of unaged arrester.

| Case | Voltage (kV) | |
|--------|--------------|--------|
| | 10.0 | 11.0 |
| Case 1 | 48.39 | 129.48 |
| Case 2 | 57.51 | 129.96 |
| Case 3 | 49.12 | 127.85 |

For each case in Table 2.2 [column #3], the applied voltage was adjusted to 11.0 kV rms. After recording data it was found that the actual voltages were 11.18, 11.22 and 11.05 kV rms for the 3 cases respectively. The conclusion is that the effect of off-centering on the diagnostic indicator is minimal and that the error can be ignored.

A similar conclusion was arrived at by examining the data obtained at a voltage of 10.0 kV rms. In this case recorded voltages were 10.01, 10.31 and 10.17 kV rms for the 3 cases respectively.

CHAPTER 3 Influence of Hysteretic $v-i_r$ Characteristics on Diagnostics

The degradation of Metal Oxide Surge Arresters (MOSA) in service is diagnosed by using the third harmonic content of the resistive portion of the arrester leakage current as an indicator. The third harmonic content consists of two components, i.e., a component due to the nonlinear volt-ampere characteristics of the MOSA and an error component due to the presence of voltage harmonics.

In order to assess the discerning ability of an on-site diagnostic method to the error component its indicator has to be compared with that of a benchmark method [20]. This chapter discusses such a method.

3.1 Introduction

As discussed in Chapter 2, a MOSA can be modeled as a nonlinear resistive element in parallel with a capacitive element. The total leakage current comprises of capacitive and resistive currents. The third harmonic content of the resistive component, $I_{3r(NL+h)}$, arises due to two reasons [14]: the nonlinear characteristics of the resistive element (identified

by the letters NL in $I_{3r(NL+h)}$), and secondly due to the presence of harmonics in the system voltage (identified by the letter h in $I_{3r(NL+h)}$). The third harmonic component due to the presence of voltage harmonics depends on the phase and the magnitude of voltage harmonics. Essentially this component is impacted by a change in the peak of the applied voltage and its shape.

When using a diagnostic method to determine the condition of a MOSA, it is important to know whether it measures the true third harmonic component, $I_{3r(NL)}$, arising solely due to the nonlinear $v-i_r$ relation of the MOSA. If not, it may be of some benefit to have knowledge of the error arising due to the difference between $I_{3r(NL)}$ and $I_{3r(NL+h)}$.

In this chapter, a method is proposed to assess the discerning ability of a diagnostic method to the error component. The proposed method involves the experimental determination of the volt-ampere characteristics of an arrester followed by a simulation procedure which calculates the third harmonic currents, $I_{3r(NL)}$ and $I_{3r(NL+h)}$. This information together with the third harmonic current obtained from a diagnostic method enables one to assess it.

3.2 Evaluation of Discerning Ability of a Diagnostic Indicator

This proposed method is explained by application to two metal oxide transmission class valve elements in series. The MCOV of this arrangement is 11 kV_{rms}, which is considered to be 1.0 p.u. throughout this chapter. The procedure is explained in the following sections.

3.2.1 Evaluation procedure

A Derivation of $v-i_r$ characteristics

As discussed in Chapter 2, hysteretic $v-i_r$ characteristics for different voltages were obtained. One such graph shown in Fig. 3.1. The voltage considered in deriving the characteristic in Fig. 3.1 includes harmonics.

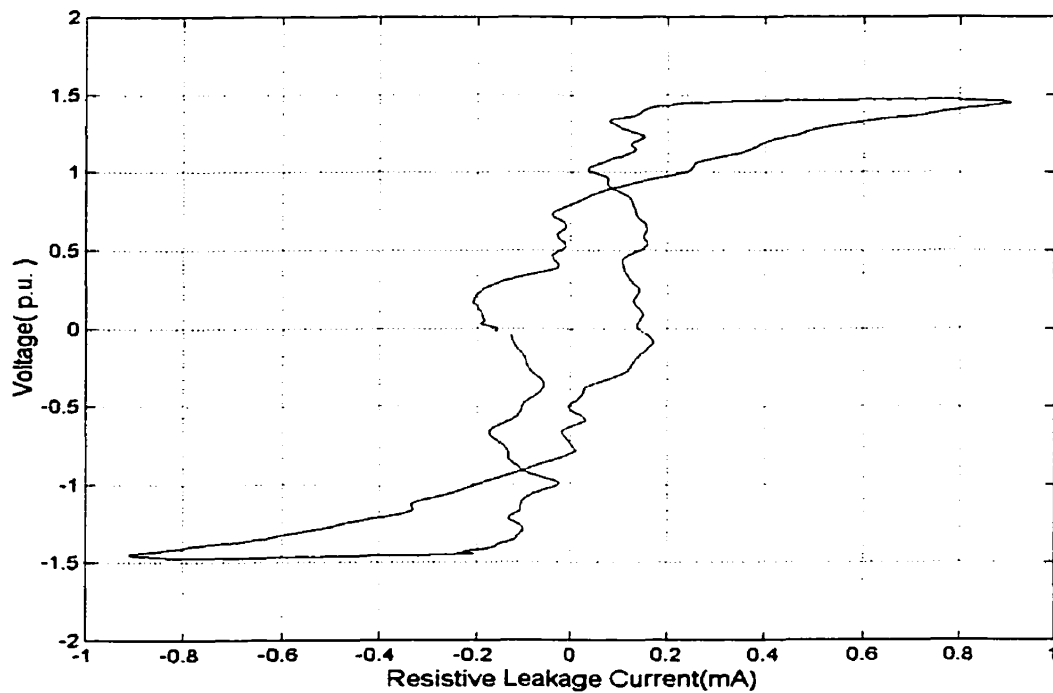


Fig. 3.1 $v-i_r$ characteristics of MO valve element

This characteristic, which is hysteretic in nature, is the true voltage-current characteristic of the two valve elements considered in this work.

B I_r due to nonlinear characteristics

The characteristic in Fig. 3.1 depends on the peak value of the applied voltage but is independent of the harmonic content of the voltage i.e. although I_r depends on the harmonic content of the applied voltage, its voltage-current characteristics are independent of harmonic content but depend on the peak value of the voltage. Based on above premise, the characteristic in Fig. 3.1 can be used to obtain $I_{3r(NL)}$. In this procedure the $v-i_r$ characteristic is represented as a look-up table where voltage is the input and the output is I_r . The I_r due to nonlinear effect only may be found by using a pure discretized sine wave as input.

Table 3.1 Tabulation of current $I_{3r(NL+h)}$ and $I_{3r(NL)}$ at various voltages

| Voltage [kV]rms | Vpeak [p.u.] | $I_{3r(NL+h)}$ [mA]rms | $I_{3r(NL)}$ [mA]rms | Error % |
|-----------------|--------------|------------------------|----------------------|---------|
| 10.50 | 0.953 | 0.0665 | 0.0704 | 5.54 |
| 10.60 | 0.963 | 0.0690 | 0.0735 | 6.12 |
| 10.70 | 0.969 | 0.0763 | 0.0819 | 6.84 |
| 10.80 | 0.983 | 0.0898 | 0.0956 | 6.07 |
| 10.90 | 0.993 | 0.0960 | 0.1004 | 4.38 |
| 11.00 | 1.000 | 0.0975 | 0.1035 | 5.80 |
| 11.10 | 1.009 | 0.1141 | 0.1188 | 3.96 |
| 11.20 | 1.019 | 0.1252 | 0.1308 | 4.28 |
| 11.30 | 1.034 | 0.1314 | 0.1432 | 8.24 |
| 11.40 | 1.041 | 0.1523 | 0.1603 | 4.99 |
| 11.50 | 1.047 | 0.1876 | 0.1950 | 3.79 |

C Obtaining the diagnostic indicator

Fourier analysis is performed on the I_r obtained in the previous step and on the I_r from experimental data. Table 3.1 gives the results of comparison of the diagnostic indicator.

The diagnostic indicator obtained experimentally is shown in the column 3. Column 4 shows the diagnostic indicator obtained by simulation which used a discretized pure sine wave as the input.

3.2.2 Discussion

Table 3.1 shows the results at various voltages in the range of 0.953 to 1.047 p.u. The difference between $I_{3r(NL)}$ and $I_{3r(NL+h)}$ as a percent of $I_{3r(NL)}$ is listed in the Table 3.1.

The error is positive and depends on the harmonic content of the voltage which, in the laboratory set-up, was not constant. For example the 3rd, 5th, and 7th harmonics at a voltage of 1.034 p.u. were 0.33%, 2.72% and 1.39% respectively; at 1.047 p.u. of voltage the corresponding values were 0.18%, 2.32% and 0.87% respectively.

It is very important that the peak of the discretized voltage should be exactly equal to the peak of the applied voltage used in the experiments to arrive at the particular $v-i_r$ plot. If this is not the case the resulting current waveform will be erroneous because of abrupt changes at the peak of the applied voltage where the slope changes sign.

3.3 Investigation of Influence of Voltage Harmonics on the Diagnostic Indicator

As pointed out earlier, the $v-i_r$ characteristic derived in the previous section [See "Derivation of v-ir characteristics" on page 27.] is the true $v-i_r$ characteristic of the device. The influence of harmonics on the diagnostic indicator can be examined by simulation. Voltage waveforms with known harmonic content were generated digitally. Third, fifth and

angles with respect to the fundamental are 180, 0, and 90 degrees respectively. These values were chosen because the results of previous work [4] and the present effort indicate that the effects of the voltage harmonics are most pronounced at these phase angles. For each voltage waveform the corresponding resistive current waveform is obtained from the $v-i_r$ characteristics.

Table 3.2 Simulation results showing effect of voltage harmonics on the diagnostic indicator

| V_{peak} [p.u.] | Voltage harmonics [%] | | | $I_{3r(\text{NL})}$ [mA]rms | $I_{3r(\text{NL+h})}$ [mA]rms | Error % |
|-----------------------------|-----------------------|------|------|--------------------------------|----------------------------------|------------|
| | 3rd | 5th | 7th | | | |
| 0.953 | | | | 0.0704 | | |
| | 0.50 | 0.50 | 0.49 | | 0.0702 | -0.28 |
| | 1.00 | 1.01 | 1.00 | | 0.0702 | -0.28 |
| | 1.50 | 1.51 | 1.50 | | 0.0701 | -0.43 |
| | 2.49 | 2.41 | 2.50 | | 0.0695 | -1.29 |
| 1.000 | | | | 0.1035 | | |
| | 0.50 | 0.50 | 0.49 | | 0.1038 | 0.29 |
| | 1.00 | 1.01 | 1.00 | | 0.1036 | 0.10 |
| | 1.50 | 1.51 | 1.50 | | 0.1029 | -0.58 |
| | 2.49 | 2.41 | 2.50 | | 0.1003 | -3.19 |
| 1.047 | | | | 0.1950 | | |
| | 0.50 | 0.50 | 0.49 | | 0.1939 | -0.57 |
| | 1.00 | 1.01 | 1.00 | | 0.1918 | -1.67 |
| | 1.50 | 1.51 | 1.50 | | 0.1888 | -3.28 |
| | 2.49 | 2.41 | 2.50 | | 0.1822 | -7.03 |

Harmonic analysis of the current waveform yields $I_{3r(\text{NL+h})}$. This is compared with $I_{3r(\text{NL})}$ found by harmonic analysis of the resistive current obtained by consideration of a pure sinusoidal voltage as explained earlier. Table 3.2 shows the results obtained.

It is seen that the voltage-harmonic induced error varies over a wide range of values from negative to positive. At a particular value of applied voltage the error increases as the harmonic content increases. For the same harmonic content the error generally increases as the applied voltage magnitude increases.

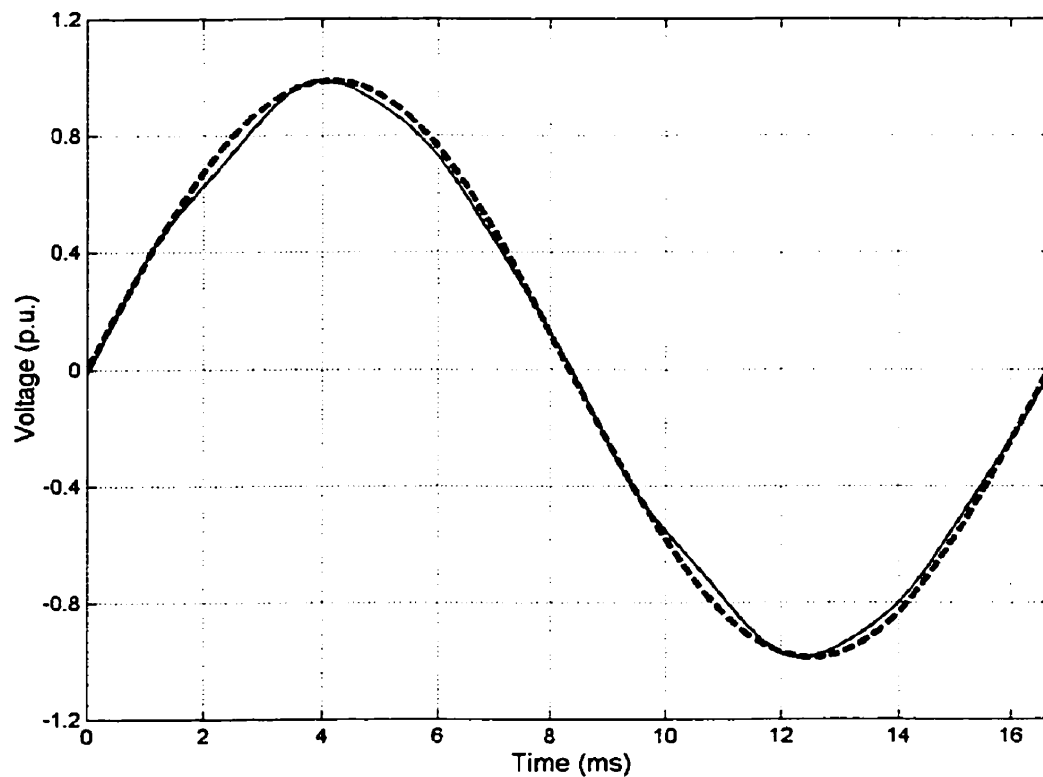


Fig. 3.2 Applied voltage. Continuous curve is contaminated with harmonics and the other is pure sine wave.

As an arrester ages its resistive current increases and the effect of voltage harmonics will be similar to that shown in Table 3.2 as the applied voltage is increased. Fig. 3.2 shows waveforms of applied voltage for the harmonic contaminated and pure sinusoidal voltage

of peak value 1.0 p.u. The 3rd, 5th, and 7th harmonics in the harmonic contaminated voltage were 1.50%, 1.51% and 1.50% respectively

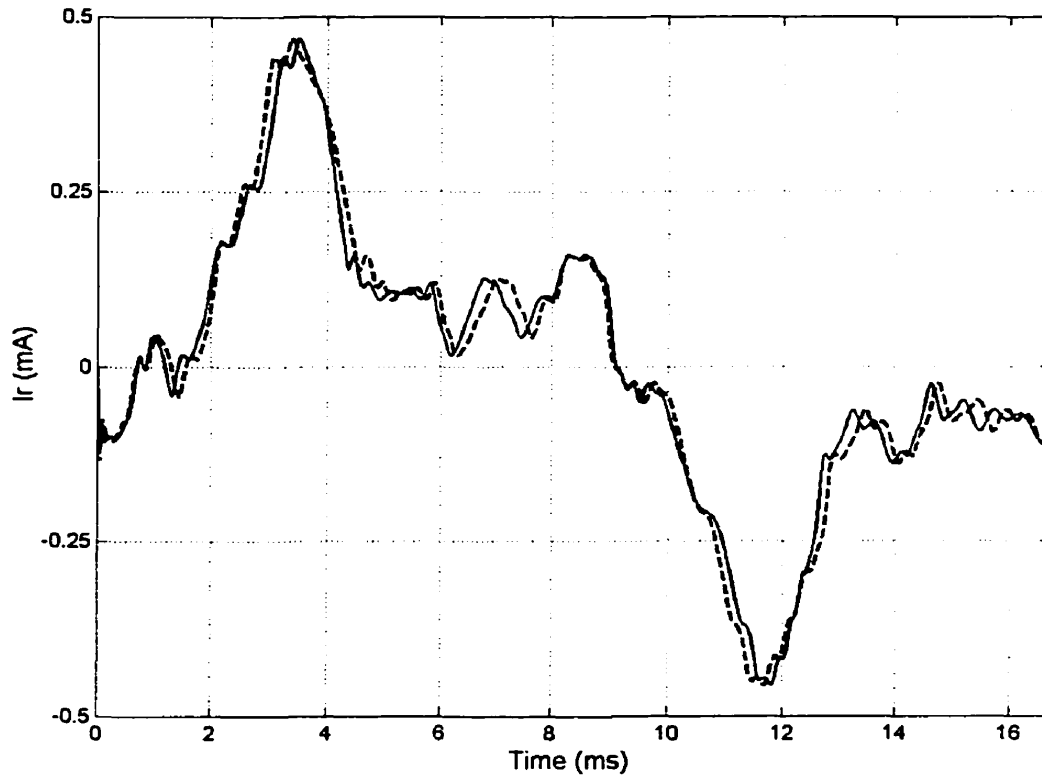


Fig. 3.3 Resistive current corresponding to harmonic contaminated voltage (thin continuous line) and pure sine voltage.

Fig. 3.3 shows resistive currents corresponding to applied voltages shown in Fig. 3.2.

The method discussed in this section allows one to obtain a diagnostic indicator which is independent of the harmonics in the applied voltage. This could be used as a benchmark to evaluate the performance of other diagnostic tools under harmonics contaminated voltages.

The drawback of this method is that it requires knowledge of applied voltage and this imposes a limitation on the application of the technique. However for new and used MOSA, diagnostic tests are carried out in laboratories (e.g. Manitoba Hydro Test Lab) and this method could be used under such conditions.

CHAPTER 4 Modeling Technique of MO Surge Arrester Including Stray Capacitance

A Metal Oxide Surge Arrester consists of a stack of valve elements mounted in a sealed housing. This chapter deals with modeling of a 115 kV arrester considering stray capacitance to ground.

4.1 MOSA without Stray Capacitance

A porcelain arrester rated at 115 kV is considered which consists of 14 MO valve elements in series; the relative permittivity of each valve element is approximately 500. The model considered in the simulation is shown in Fig. 4.1(a). Each valve element pair is considered as a unit and each unit is modelled as discussed in Chapter 2 [Fig.4.1(b)]. The resistance of the MOSA varies with instantaneous applied voltage and its nonlinear characteristics are governed by the simplified $v-i_r$ characteristic shown in Fig. 4.1(c). The capacitance varies with applied voltage as well but it is not significant, and it is assumed to be constant at a value of 275pF. Without stray capacitance, the voltage distribution along the arrester is uniform.

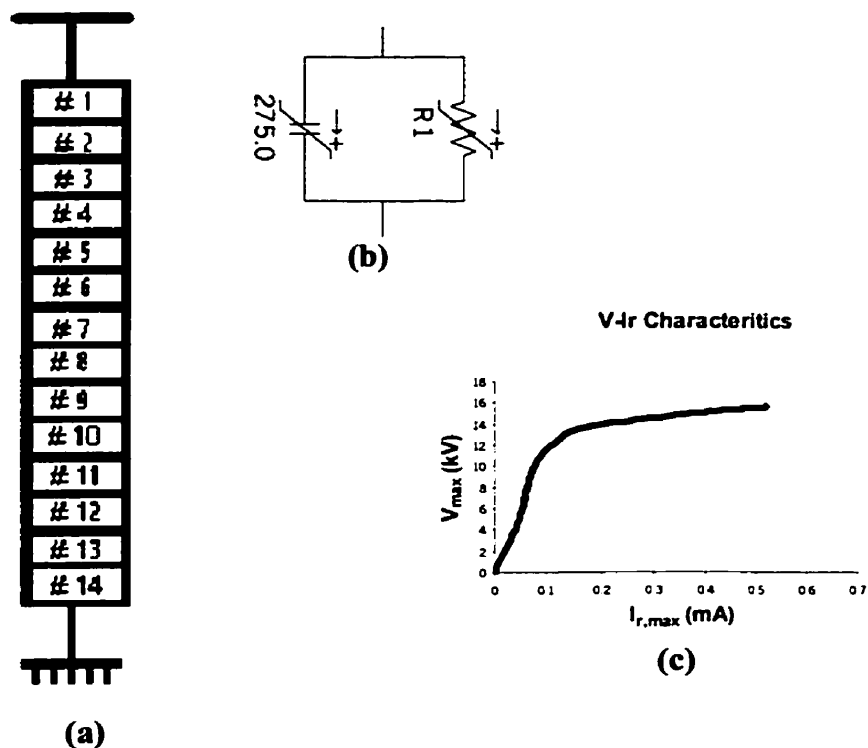


Fig. 4.1 MOSA without strays

4.2 MOSA with Stray Capacitance

The distribution of stray capacitance was considered as shown in Fig. 4.2. The MOSA

Table 4.1 Stray capacitances considered in the simulation

| | Cg20 [pF] | Cg30 [pF] | Cg40 [pF] | Cg50 [pF] | Cg60 [pF] |
|-----|-----------|-----------|-----------|-----------|-----------|
| CS1 | 1.75 | 1.75 | 1.75 | 1.75 | 1.75 |
| CS2 | 2.25 | 2.25 | 2.25 | 2.25 | 2.25 |
| DS1 | 1.75 | 1.68 | 1.61 | 1.54 | 1.47 |
| DS2 | 2.25 | 2.16 | 2.07 | 1.98 | 1.89 |

considered in this work does not have a grading ring, thus stray capacitance to high voltage conductor can be ignored.

Table 4.1 gives the stray capacitance values for the different cases considered in the simulation. The symbols DS1 and DS2 stand for the cases where the stray capacitance is considered to be distributed and their values are given in Table 4.1. The strays Cg20 through Cg60 indicates capacitance values from various nodes to ground and are shown in Fig. 4.2. The symbols CS1 and CS2 stand for the cases where the stray capacitance is considered to be constant. The capacitance value corresponding to the first column (Cg20) of DS1 is taken as the constant stray capacitance value of CS1. Similarly, the value of CS2 is selected from DS2.

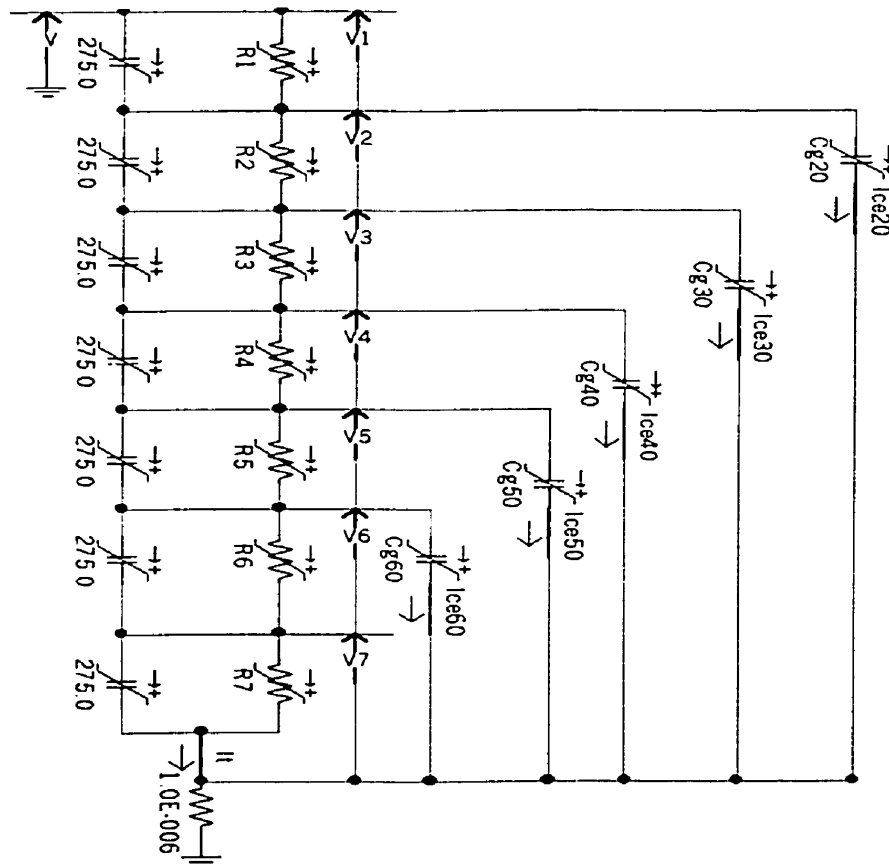


Fig. 4.2 MOSA with strays

The values for cases DS1, DS2 were selected on the basis of previous work [5, 21]. In [21] the earth capacitances of the arrester were determined by measuring the axial current distribution along the arrester column. This was done by specially designed, battery powered current sensors with signal transmission to earth by fibre optic cable. The sensors have the same dimensions as a single MO disk and can be placed anywhere in the arrester column instead of a MO disk. For the measurement a voltage much less than the normal operating voltage was applied to the arrester so that the resistance and the capacitance of the MO disks can be assumed to be linear elements. Inserting their values into the electrical equivalent circuit [21], the distribution of earth capacitance of the arrester column can be determined from the measured current distribution.

In [5] the voltage distribution of the arrester was arrived at numerically based on the finite element method. The authors found that the axial voltage distribution along the MO valve element column became more non-uniform with decrease of permittivity. More over, the voltage distribution of the arrester with composite housing was slightly non-uniform than that with porcelain housing. Thus voltage distribution along the arrester is influenced by the permittivity and type of housing selected.

The selected variation in the stray capacitance values [Table 4.1 on page 35] agrees with that reported in [21]. In cases CS1 and CS2 the capacitance values were selected to be equal to that from the top most node i.e. C_{g20} in cases DS1 and DS2 respectively. Comparison of results yields the effect of a distributed capacitance on the diagnostic indicator.

The presence of stray capacitance introduces a non-uniform voltage distribution. The resistance of the non-linear resistive element changes with voltage. The voltage distribution is determined not only by capacitances but also by the value of resistance. Therefore finding the correct value R , poses quite a challenge. In this thesis an iterative method has been developed and the algorithm is shown in Fig. 4.3.

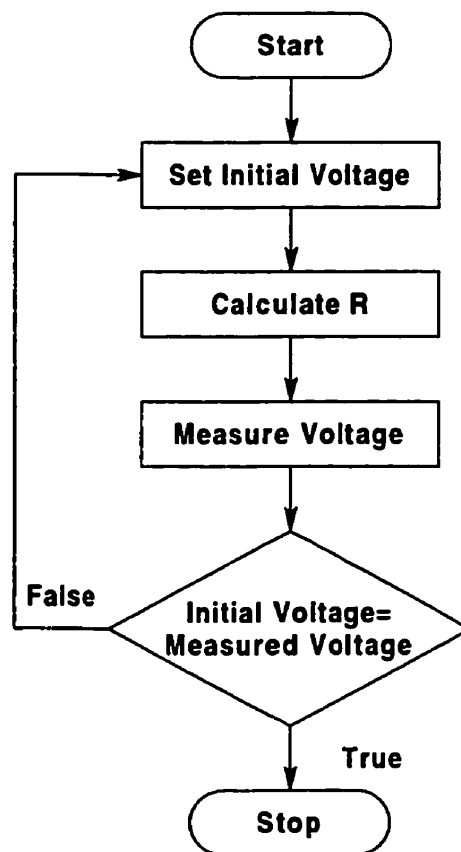


Fig. 4.3 Algorithm used in calculating resistive element R

In the simulation process the solution is initiated by choosing suitable values for the voltages across valve element pairs following which the program computes the actual voltage

distribution and the voltage across each valve element taking into account the presence of stray capacitances. These values are then used as the valve element voltages in the next iteration. This procedure is repeated until convergence is achieved.

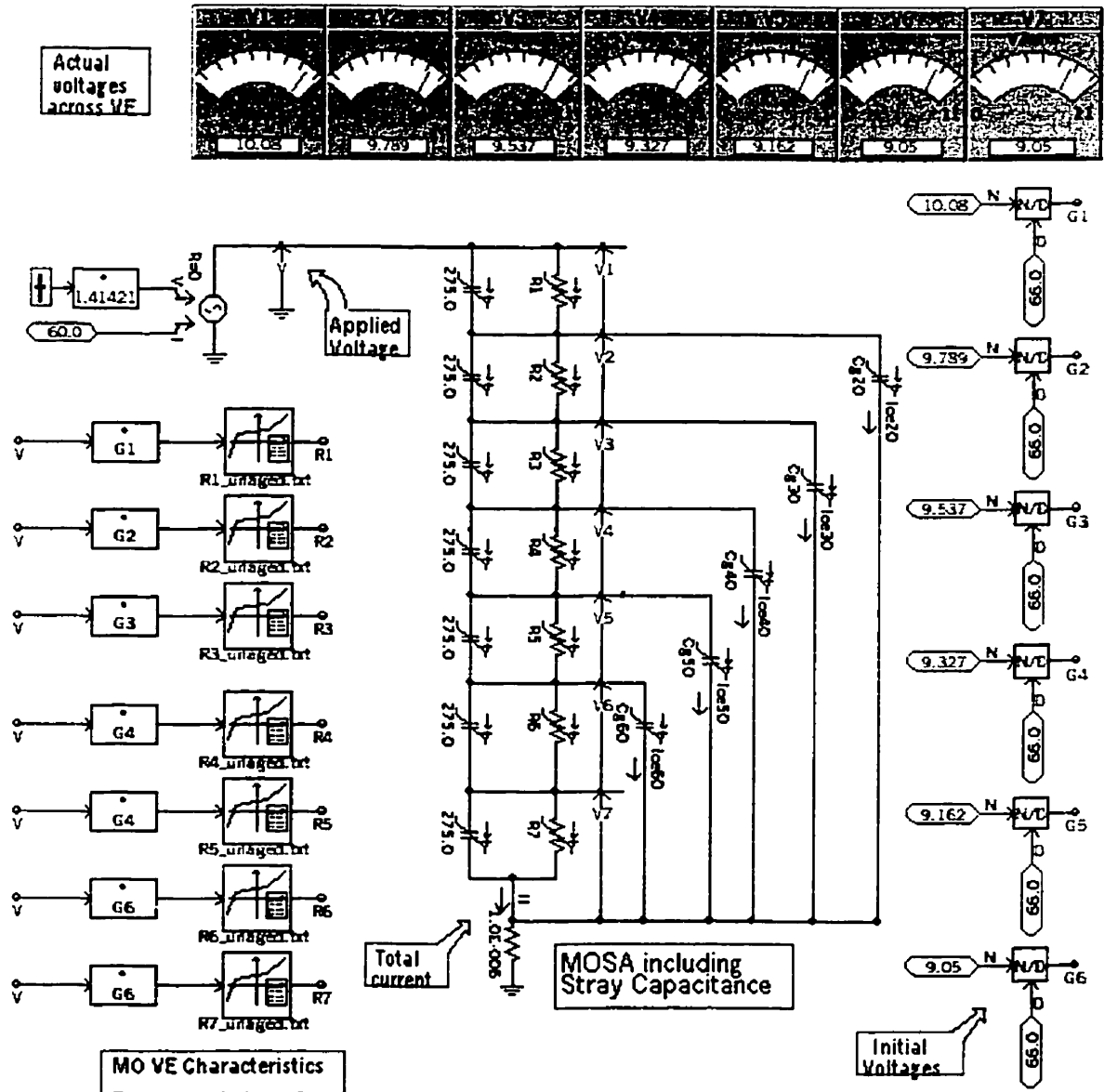


Fig. 4.4 PSCAD case

Fig. 4.4 shows a PSCAD case used in this simulation which corresponds to the final iteration where initial and actual computed values are the same. The section labelled “MO VE Characteristics” are data files that determine the nonlinear resistance of the valve elements. In each valve element there is an individual data file labelled as Ri_unaged.txt ($i = 1..7$). For this particular example only unaged characteristics are considered. By changing the text file, the characteristics of the individual valve elements can be changed. Control elements labeled “Initial Voltages” correspond to the initial guess value of the voltage across the valve element i.e. 10.08 kV for top valve element and 9.05 kV for bottom valve element. The graphical meters, “Actual voltage across VE”, show the computed voltages across the individual valve elements. In this particular case computed values are the same as initial voltages thus the iterative process has converged.

Table 4.2 Voltage across the MO valve elements

| Voltage across the VE [Fig. 4.4] | Initial Voltage (kV) _{rms} | Iteration | | |
|-------------------------------------|--|-----------|-------|-------|
| | | #1 | #2 | #3 |
| V1 | 9.429 | 10.09 | 10.08 | 10.08 |
| V2 | 9.429 | 9.492 | 9.789 | 9.789 |
| V3 | 9.429 | 9.536 | 9.537 | 9.537 |
| V4 | 9.429 | 9.324 | 9.327 | 9.327 |
| V5 | 9.429 | 9.159 | 9.162 | 9.162 |
| V6,V7 | 9.429 | 9.045 | 9.050 | 9.050 |

Table 4.2 shows the complete results of the 3 iterations which converged to voltages as seen in Fig. 4.4. In this example we have considered the applied voltage across the arrester to be a pure sinusoid, and a case where all the valve elements are unaged and stray capacitance distribution is as per row 3 in Table 4.1 i.e. DS1. Initially it is assumed that the volt-

age distribution across the arrester is uniform i.e. voltage across each valve element is 9.429 kV. Those voltages are shown in column 1. Let us consider voltage across the first valve element pair (top most valve elements in Fig. 4.4 on page 39). For a uniform voltage distribution, $V_1=9.429$ kV. After running the simulation for 1 sec. with a time step of 50 μ s, the actual voltage computed for each valve element is shown in column 3 (i.e. iteration #1). The voltage across the top most valve element, V_1 , is now 10.09 kV. This indicates that the initial guess was wrong and further iterations are required. Now, the initial voltages are replaced by values computed in the first iteration i.e. for case of the top valve element $V_1=9.429$ is replaced by $V_1=10.09$ kV. This procedure is repeated for all the valve elements. After each iteration the actual values computed in the simulation become initial voltages for the next simulation. This process is repeated until the initial and actual computed voltages are the same. As shown in Table 4.2, after 3 iterations the initial and computed actual voltages are the same, and thus correct non-linear resistance values were found.

Fig. 4.3 shows the voltage distribution along the arrester for the case considered. It is seen that the selection of stray capacitance [Table 4.1 on page 35] gives rise to a voltage distribution which agrees with that in [5].

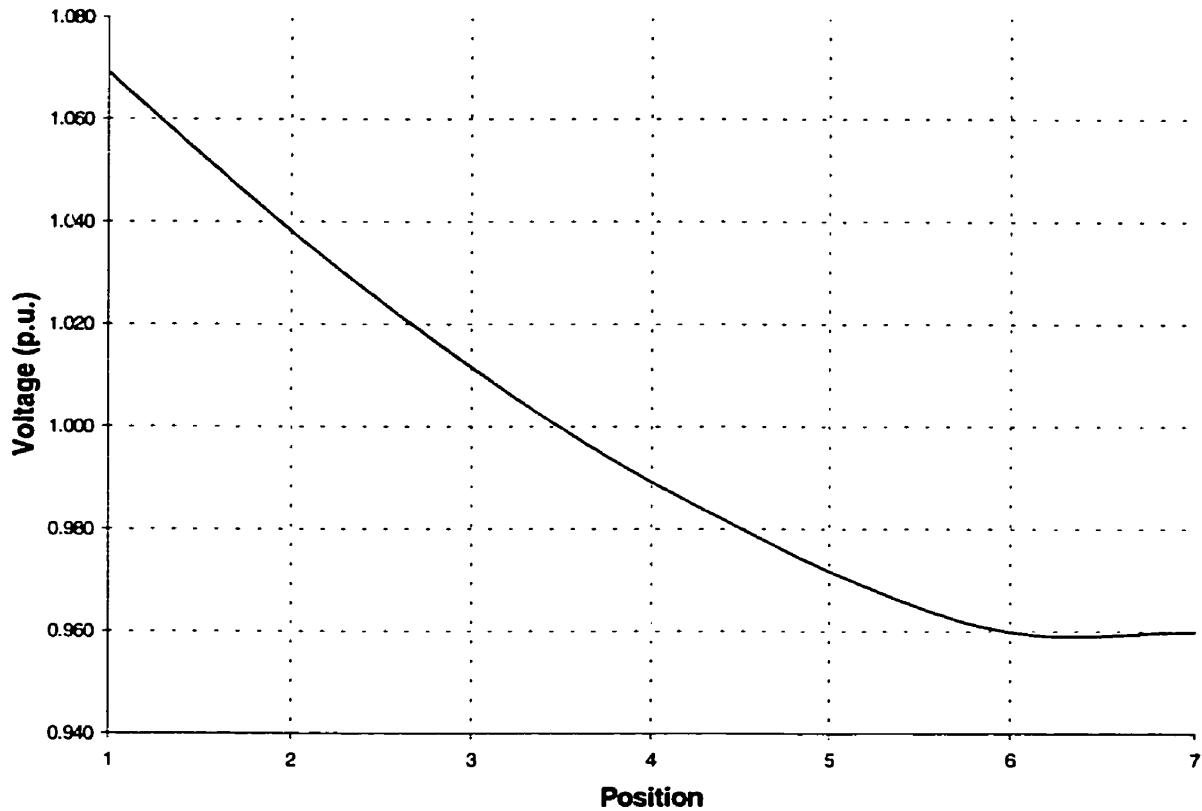


Fig. 4.5 Voltage distribution along the MOSA. 1.0 p.u. corresponds to uniform voltage distribution i.e. 9.429 kV rms.[Position 1 is the high voltage terminal]

4.3 Aging of MO Valve Element

Aging is defined as change (deterioration) of physical characteristics of the valve element during the operation [22]. Using the simulation model discussed in this chapter aging of individual valve elements can be studied. The characteristics of the resistive element change as shown in Fig. 4.6. The unaged characteristics, CH1, and the aged characteristic, CH5, were obtained experimentally as discussed in Chapter 2. The rest of the characteristics were derived using CH1 and CH5. CH3 is the average of CH1 and CH5; while CH2 is the average of CH1 and CH3.

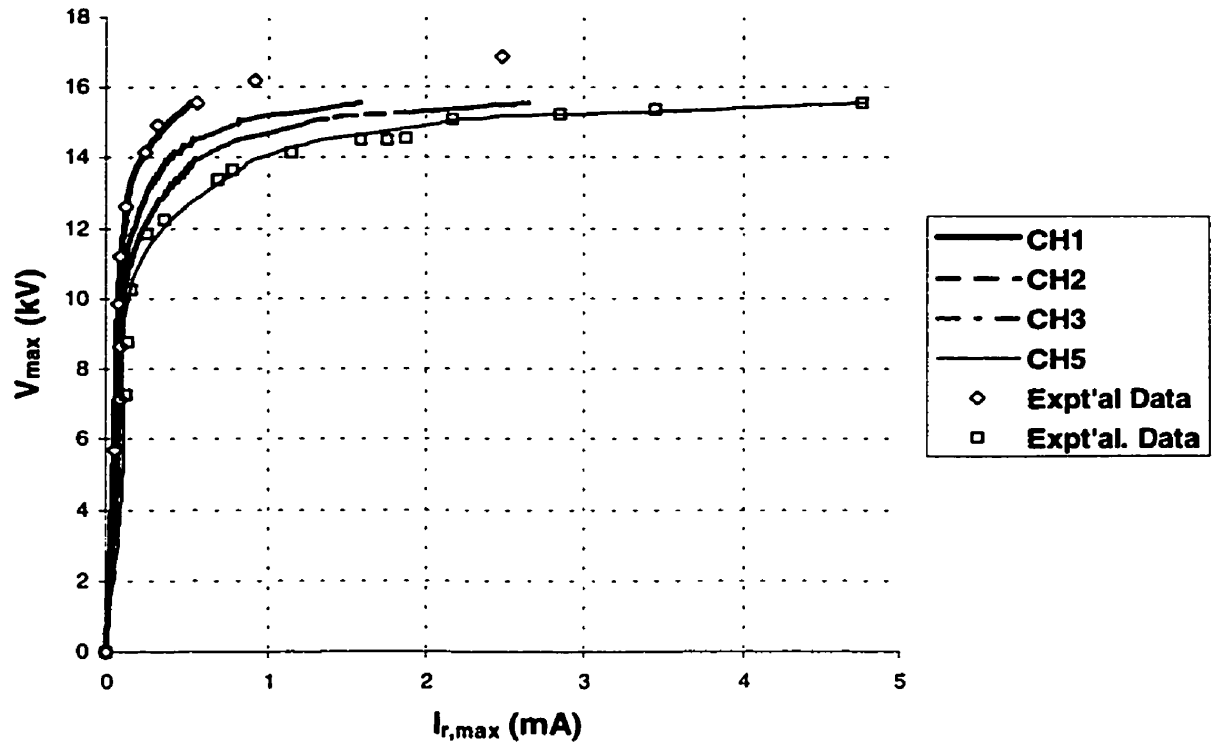


Fig. 4.6 Simplified $v-i_r$ characteristics for unaged and aged MO valve element pair

For each characteristic (CH1..CH5) a separate file was evaluated that stores data points correspond to the $v-i_r$ relation. The characteristics of any MO valve element can be changed simply by changing the file reference in “MO VE Characteristics” [Fig. 4.4 on page 39].

4.4 Simulation Procedure

Simulations were carried out using PSCAD/EMTDC™ [23]. Depending on the case considered i.e. CS1,DS1 or no stray (NS) etc., different PSCAD cases were considered. For

each case the valve element characteristics and voltage source were selected first. Next simulations were carried out using the iteration technique discussed earlier. Once the computed actual voltages converged to the initial voltages, one last simulation run was carried out. After the simulation, the voltage across the MOSA, V , and total current I_t [Fig. 4.4 on page 39] were saved into a data file. Fig. 4.7 shows example of such waveforms saved into a data file. The total voltage across the arrester in this case is 66 kV rms. Since the arrester is operated well below its maximum continuous operating voltage (MCOV) the resistive component is considerably small.

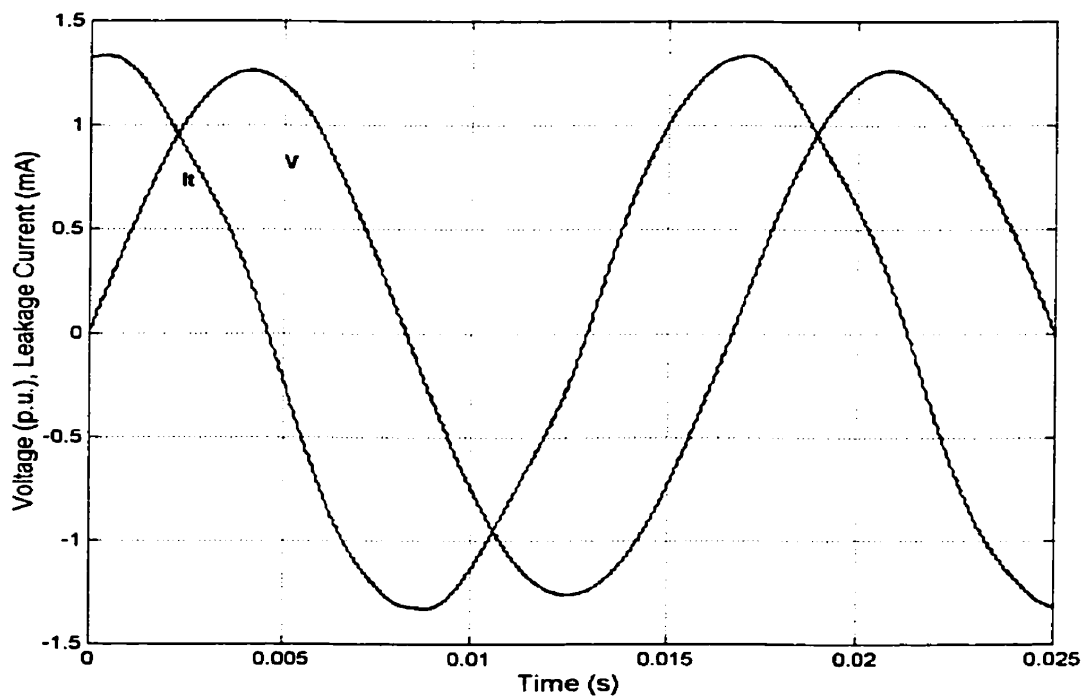


Fig. 4.7 Waveforms of arrester voltage and total arrester current from simulated results

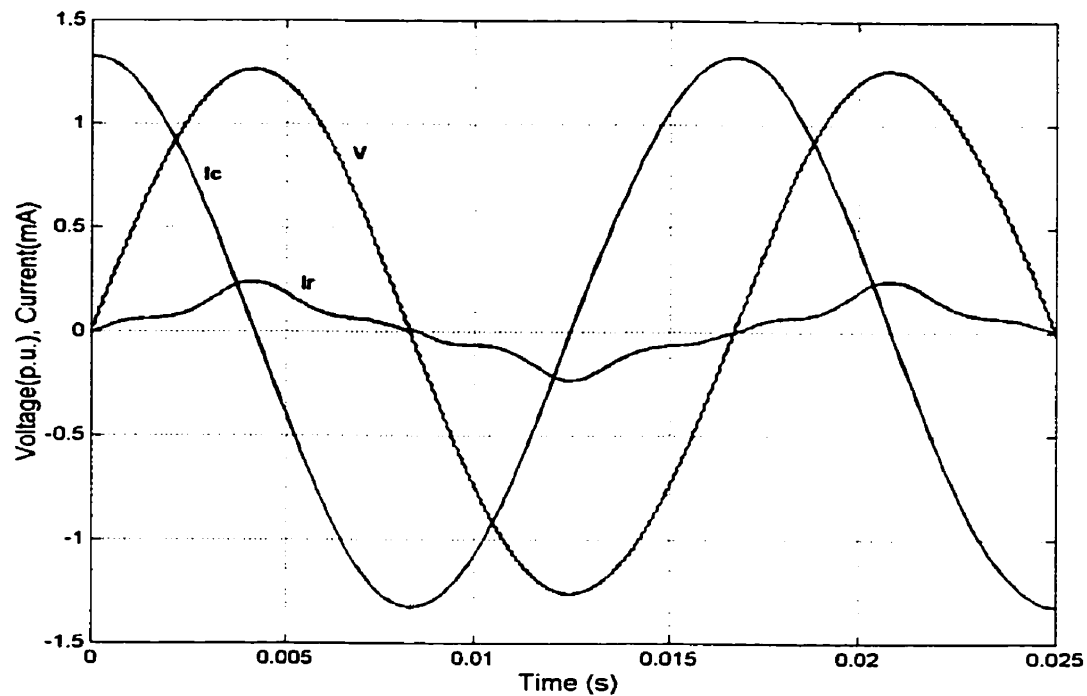


Fig. 4.8 Waveform of applied voltage, arrester capacitive and resistive currents.

Applying the Compensation Technique to the above data file, the effective capacitance is calculated. As discussed earlier [See “Derivation of v-ir Characteristics of the Resistive Element.” on page 13.] the resistive leakage current and thus diagnostic indicator can be calculated. Fig. 4.8 shows the resistive and capacitive currents which corresponds to Fig. 4.7.

CHAPTER 5 Effect of Stray Capacitance and Ageing on MOSA Diagnostic Indicator

This chapter is concerned with the results of a simulation study in which the 115 kV arrester [Fig. 4.2 on page 36] has been considered and the effects of voltage harmonics and valve element condition on the diagnostic indicator have been evaluated taking into account the presence of distributed stray capacitance by using the simulation procedure described in Chapter 4 [24].

5.1 Effect of Stray Capacitance on the Diagnostic Indicator

To evaluate the effects of stray capacitance on the diagnostic indicator the applied voltage was considered to be a pure sinusoid, valve element capacitance considered constant and unaged valve elements were considered. Five cases of stray capacitance were considered i.e. no strays (NS), constant stray capacitance (CS1, CS2), and distributed stray capacitance (DS1, DS2) [Table 4.1 on page 35]. For each of these cases the procedure described in Chapter 4 yielded the diagnostic indicator and those values are listed in Table 5.1.

Table 5.1 Effect of stray capacitance on the diagnostic indicator (μA) of unaged arrester. Voltage harmonic content nil. Stray capacitance as per Table 4.1. VE capacitance constant.

| Case | | | | |
|-------|-------|--------|-------|-------|
| NS | CS1 | CS2 | DS1 | DS2 |
| 6.559 | 9.137 | 10.627 | 8.663 | 9.878 |

It is seen that inclusion of a realistic distribution of stray capacitance (DS1 and DS2) results in an increase in the indicator of 32% to 50% over that when the strays are neglected. These results show the danger of comparing field and laboratory data on the same arrester. Comparison of the diagnostic indicator obtained with CS and DS show that the differences are small i.e. \approx 5 to 8%. These differences should be borne in mind in simulation studies.

5.2 Effect of Ageing on the Diagnostic Indicator

As stated in Chapter 2, as a MOSA ages its capacitance tends to increase. In this section it is assumed that the capacitive element of the metal oxide valve element remains constant. To evaluate the effects of ageing on the diagnostic indicator the applied voltage was considered to be pure sinusoid and valve element capacitance constant. Ageing was modelled by consideration of characteristics CH2, CH3 and CH5 [Fig. 4.6 on page 43].

5.2.1 Only one valve element pair is aged

There are 7 valve element pairs in the simulated MOSA. The results in this section consider only one element pair to be aged. The location of the aged pair was varied. Five locations have been considered i.e. VE #1 & #2 [Fig. 2.2 on page 13], VE #3 & #4 etc. For

each case five cases of stray capacitance distributions were considered as outlined in Table 5.1.

Table 5.2 Effect of ageing of VE #1 & #2 on the diagnostic indicator (μA). Voltage harmonic content nil. Stray capacitance as per Table 4.1. VE capacitance constant

| Valve element characteristics | Case | | | | |
|-------------------------------|--------|--------|--------|--------|--------|
| | NS | CS1 | CS2 | DS1 | DS2 |
| CH2 | 9.930 | 15.224 | 18.395 | 14.365 | 16.535 |
| CH3 | 13.116 | 21.067 | 25.905 | 19.712 | 22.918 |
| CH4 | 16.142 | 26.685 | 33.870 | 24.982 | 29.517 |
| CH5 | 19.007 | 32.513 | n/a | 30.041 | 36.037 |

Table 5.3 Effect of ageing of VE #3 & #4 on the diagnostic indicator (μA). Voltage harmonic content nil. Stray capacitance as per Table 4.1. VE capacitance constant.

| Valve element characteristics | Case | | | | |
|-------------------------------|--------|--------|--------|--------|--------|
| | NS | CS1 | CS2 | DS1 | DS2 |
| CH2 | 9.930 | 13.886 | 15.669 | 13.866 | 14.744 |
| CH3 | 13.116 | 18.325 | 20.418 | 18.325 | 19.385 |
| CH4 | 16.142 | 22.624 | 25.017 | 22.264 | 23.985 |
| CH5 | 19.007 | 26.854 | 29.570 | 26.854 | 28.391 |

Table 5.4 Effect of ageing of VE #5 & #6 on the diagnostic indicator (μA). Voltage harmonic content nil. Stray capacitance as per Table 4.1. VE capacitance constant

| Valve element characteristics | Case | | | | |
|-------------------------------|--------|--------|--------|--------|--------|
| | NS | CS1 | CS2 | DS1 | DS2 |
| CH2 | 9.930 | 12.859 | 14.506 | 12.397 | 13.717 |
| CH3 | 13.116 | 16.419 | 18.090 | 15.971 | 17.395 |
| CH4 | 16.142 | 19.828 | 21.580 | 19.385 | 20.910 |
| CH5 | 19.007 | 23.058 | 24.930 | 22.633 | 24.258 |

Table 5.5 Effect of ageing of VE #7 & #8 on the diagnostic indicator (μA). Voltage harmonic content nil. Stray capacitance as per Table 4.1. VE capacitance constant

| Valve element characteristics | Case | | | | |
|-------------------------------|--------|--------|--------|--------|--------|
| | NS | CS1 | CS2 | DS1 | DS2 |
| CH2 | 9.930 | 12.019 | 13.380 | 11.627 | 12.736 |
| CH3 | 13.116 | 14.830 | 16.083 | 14.497 | 15.463 |
| CH4 | 16.142 | 17.500 | 18.655 | 17.172 | 18.119 |
| CH5 | 19.007 | 20.022 | 21.019 | 19.736 | 20.632 |

Table 5.6 Effect of ageing of VE #9 & #10 on the diagnostic indicator (μA). Voltage harmonic content nil. Stray capacitance as per Table 4.1. VE capacitance constant

| Valve element characteristics | Case | | | | |
|-------------------------------|--------|--------|--------|--------|--------|
| | NS | CS1 | CS2 | DS1 | DS2 |
| CH2 | 9.930 | 12.128 | 13.487 | 11.733 | 12.847 |
| CH3 | 13.116 | 15.219 | 16.473 | 14.887 | 15.847 |
| CH4 | 16.142 | 18.355 | 19.500 | 18.030 | 18.974 |
| CH5 | 19.007 | 21.546 | 22.519 | 21.359 | 22.166 |

For any chosen nature of stray capacitance i.e. NS, CS1, etc. the diagnostic indicator increases as ageing is considered. For example when VE #1 & #2 are considered to have aged considerably i.e. characteristics CH5, and the stray capacitance distribution is DS2, the diagnostic indicator changes by approximately 265%[†]. This is the worst change; the least change i.e. 109%, occurs when VE #7 & #8 are similarly aged stray capacitance corresponds to DS2[‡]. A similar trend is evident for all the cases reported when values in Table 5.1 are compared with corresponding values in Table 5.2 to 5.6.

[†] From Tables 5.1 and 5.2 (36.037-9.878)/9.878%

[‡] From Tables 5.1 and 5.5 (20.632-9.878)/9.878%

For any chosen nature of stray capacitance variation ageing of top most pair (VE #1 & #2) results in the greatest increase in the diagnostic indicator. As the location of the aged pair is shifted down the arrester column the increase in the diagnostic indicator becomes less. There is a slight increase in the diagnostic indicator when VE #9 & #10 are aged compared to the valve element pair just above. Transfer of voltage across the other elements in the top of the column is more pronounced in this case as opposed to the case where VE #7 & #8 are aged.

5.2.2 Multiple valve elements are aged

The following table shows the effect of aging of more than one valve element pair. The location of the first pair and its $v-i_r$ characteristics are identified in the first two columns and that of the second aged pair identified in the third and fourth columns. The distribution of stray capacitance considered corresponds to NS, DS2 and CS2 [Table 4.1 on page 35]. The applied voltage was considered to be a pure sinusoid and the valve element capacitance considered constant.

Table 5.7 Effect of ageing of four VE's on the diagnostic indicator (μA). Voltage harmonic content nil. Stray capacitance as per Table 4.1. VE capacitance constant

| First VE pair | | Second VE pair | | Case | | |
|---------------|----------|----------------|----------|--------|--------|--------|
| VE # | Charact. | VE # | Charact. | NS | DS2 | CS2 |
| 1,2 | CH2 | 3,4 | CH2 | 13.328 | 21.424 | 23.234 |
| 1,2 | CH2 | 5,6 | CH2 | 13.328 | 20.422 | 22.101 |
| 1,2 | CH2 | 7,8 | CH2 | 13.328 | 19.432 | 21.036 |
| 3,4 | CH2 | 5,6 | CH2 | 13.328 | 18.656 | 19.498 |
| 3,4 | CH2 | 7,8 | CH2 | 13.328 | 17.675 | 18.436 |
| 5,6 | CH2 | 7,8 | CH2 | 13.328 | 16.598 | 17.281 |
| 1,2 | CH2 | 3,4 | CH3 | 16.538 | 26.089 | 28.094 |

Table 5.7 Effect of ageing of four VE's on the diagnostic indicator (μA). Voltage harmonic content nil. Stray capacitance as per Table 4.1. VE capacitance constant

| First VE pair | | Second VE pair | | Case | | |
|---------------|----------|----------------|----------|--------|--------|--------|
| VE # | Charact. | VE # | Charact. | NS | DS2 | CS2 |
| 1,2 | CH2 | 5,6 | CH3 | 16.538 | 24.053 | 25.881 |
| 1,2 | CH2 | 7,8 | CH3 | 16.538 | 22.198 | 23.711 |
| 3,4 | CH2 | 5,6 | CH3 | 16.538 | 22.350 | 23.161 |
| 3,4 | CH2 | 7,8 | CH3 | 16.538 | 20.420 | 21.156 |
| 5,6 | CH2 | 7,8 | CH3 | 16.538 | 19.410 | 19.437 |
| 1,2 | CH3 | 3,4 | CH3 | 19.783 | 32.499 | 35.482 |
| 1,2 | CH3 | 5,6 | CH3 | 19.783 | 30.573 | 33.308 |
| 1,2 | CH3 | 7,8 | CH3 | 19.783 | 28.715 | 31.294 |
| 3,4 | CH3 | 5,6 | CH3 | 19.783 | 27.048 | 27.977 |
| 3,4 | CH3 | 7,8 | CH3 | 19.783 | 25.131 | 25.981 |
| 5,6 | CH3 | 7,8 | CH3 | 19.783 | 23.137 | 23.660 |
| 1,2 | CH3 | 3,4 | CH2 | 16.538 | 27.862 | 30.728 |
| 1,2 | CH3 | 5,6 | CH2 | 16.538 | 26.879 | 29.610 |
| 1,2 | CH3 | 7,8 | CH2 | 16.538 | 25.894 | 28.545 |
| 3,4 | CH3 | 5,6 | CH2 | 16.538 | 23.335 | 24.278 |
| 3,4 | CH3 | 7,8 | CH2 | 16.538 | 22.358 | 23.218 |
| 5,6 | CH3 | 7,8 | CH2 | 16.538 | 20.299 | 20.898 |

For stray capacitance variations corresponds to CS2 and DS2 ageing of top two pairs (VE #1, #2, #3 & #4) result in the greatest increase in the diagnostic indicator. For example, with slightly aged valve elements (i.e. characteristic CH2) the diagnostic indicator increases by 117% when the stray capacitance distribution is DS2. As the location of the aged pairs are shifted down the arrester column, the increase in the diagnostic indicator becomes less. In the case of ageing of VE #5 to #8 (i.e. characteristic CH2) the diagnostic indicator increased by 68% only when the stray capacitance distribution is DS2. This trend is common to all the cases reported in Table 5.7. For stray capacitance distributions corre-

sponding to CS2 and DS2 the percent increase in the diagnostic indicator due to ageing is the same.

5.3 Effect of Harmonics on the Diagnostic Indicator

For a selected number of cases, the effect of the presence of harmonics in the system voltage was simulated. The stray capacitance distribution was selected corresponding to case DS2 and valve element capacitance was considered constant. The characteristics of the valve element and its location are given in columns one and two respectively. The value of the diagnostic indicator for voltages with harmonics and without harmonics are listed in columns three and four respectively. Harmonic content was selected to reflect practical values prevalent in Manitoba Hydro's 230 kV system, i.e. 0.282%, 0.373% and 0.289% of 3rd, 5th and 7th voltage harmonics respectively.

Table 5.8 Effect of voltage harmonics on the diagnostic indicator (μA). Distributed stray capacitance as per DS2 (Table 4.1). VE capacitance constant.

| Characteristics of the VE | Location of the aged VE's | Applied Voltage | |
|---------------------------|---------------------------|-------------------|----------------|
| | | Without harmonics | With harmonics |
| CH1 | None | 9.878 | 9.669 |
| CH2 | 5,6 | 13.717 | 13.461 |
| CH2 | 3,4,5,6 | 18.656 | 18.378 |

For each case in Table 5.8, the error due to the presence of harmonics is less than 1.5%. The conclusion is that the effect of harmonics on the diagnostic indicator is minimal and that the error can be ignored in simulation studies. However if the harmonic content is significantly higher (i.e. in the range of 3 to 5%) the effect of harmonics need to be consid-

ered [14]. Furthermore in the present study simplified $v-i_r$ characteristics have been used and the characteristics are not so sensitive to harmonics in the applied voltage as would be the case where hysteretic characteristics were used [Fig. 2.5 on page 17].

5.4 Effect of Change in Capacitance of the VE due to Ageing

As discussed in Chapter 2, as a MOSA ages its capacitance increases. The following table shows the effect on the diagnostic indicator. Column one identifies the cases considered in the simulation; the location of the aged valve elements according to column two are VE #5 & #6. The characteristics of the aged valve element correspond to CH5 [Fig. 4.6 on page 43]. Column three and four list the results of the simulation study. In this study extreme case of ageing i.e. characteristics CH5, is considered when the capacitive element of the valve element changes to 290 pF from 275 pF due to ageing.

Table 5.9 Effect of change in the capacitance on the diagnostic indicator (μA). Voltage harmonic content nil. Stray capacitance as per Table 4.1.

| Case | Location of the aged VE's | Capacitive element (pF) | |
|------|---------------------------|-------------------------|---------|
| | | C=275 | C=290 |
| NS | 5, 6 | 19.0073 | 13.7943 |
| DS1 | 5, 6 | 22.6331 | 17.4967 |

It is seen that a change in capacitance results in a 25% (approx.) decrease in the diagnostic indicator. If the change in valve element capacitance with ageing is ignored in simulation studies, the diagnostic indicator obtained would be an optimistic value. For cases of slight ageing i.e. characteristics CH2, the change in capacitance is not so significant and thus it can be assumed to be constant.

5.5 Practical Significance of Simulation Results

The presence of stray capacitance leads to a non-uniform voltage distribution which in turn affect arrester diagnostics. In the presence of stray capacitance the increase in the diagnostic indicator is most pronounced where valve elements are at top of the column are aged. This increase is greater as ageing become more pronounced.

In the absence of stray capacitance (NS) the location of the aged elements have no influence on the change in the diagnostic indicator. In [5] the use of valve elements with different permittivity has been suggested with a view to improve the voltage distribution to as near uniform as possible. In this event the above conclusion applies.

When comparing field and laboratory data, one must consider the effect of harmonics and stray capacitance distribution because the field values of these parameters will not be the same as the lab values.

CHAPTER 6 Conclusions

6.1 Summary

In this thesis, effect of hysteretic $v-i_r$ characteristics, stray capacitance and voltage harmonics on the diagnostic indicator are investigated. The active part of an arrester is the MO valve elements. Chapter 2 explains how these valve elements can be modeled using a simple model valid for normal operating voltages of the arrester. The elements of this model are derived using an experimental set-up, and a numerical technique which is implemented using Matlab. Presence of harmonics in the applied voltage results in errors in the diagnostic indicator. In Chapter 3, a method is proposed to evaluate the discerning ability of the diagnostic indicator due to hysteresis character of the valve element and voltage harmonics. Metal Oxide arresters consist of a stack of valve elements mounted in a sealed housing. Chapter 4 discusses the modeling technique of MO surge arresters including stray capacitance. Finally, in Chapter 5, effects of stray capacitance and voltage harmonics on the diagnostic indicator are discussed by presenting the results of the simulation work carried out using the model discussed in Chapter 4.

6.2 Conclusions

The following conclusions may be drawn from the study in this thesis:

1. The effect of off-centering of valve elements due to the air gap between MO valve element and its casing, on the diagnostic indicator is minimal and can therefore be ignored.
2. Due to hysteretic $v-i_r$ characteristics of valve elements, the diagnostic indicator is very sensitive to harmonics in the voltage. Neglecting voltage harmonics in arrester diagnostics may lead to misleading conclusions.
3. The diagnostic indicator is influenced by the voltage distribution along the arrester column. Presence of stray capacitance result in the non-uniform voltage distribution. Therefore when comparing diagnostic indicators it is important that tests be carried out under similar conditions.
4. The diagnostic indicator is affected by the location of the aged valve element in the arrester column.
5. In the absence of stray capacitance the location of the aged valve element has no influence on the change in the diagnostic indicator.

6.3 Recommendations for Future Research

1. The possibility of incorporating the Compensation Technique in the routine test procedure used by Manitoba Hydro should be explored.
2. The effect of change in capacitance of the valve element due to ageing should be investigated.

APPENDIX A Inclusion of Compensation Technique in Manitoba Hydro Test Procedure

To monitor and evaluate the condition of MOSA, various tests are performed by Manitoba Hydro. This section deals with one such method used in their laboratory. Furthermore the possibility of using the Compensation Technique to enhance the tests carried out by Manitoba Hydro is explored.

A.1 Laboratory Test Procedure

As already discussed, ageing of MOSA results in an increase in resistive current. For new and used arresters, Manitoba Hydro conducts certain tests that can be used to evaluate the condition of the arrester. This test set-up allows the measurement of peak resistive current of the arrester using a hardware technique. The following four tests are carried out evaluate arrester condition.

1. Voltage equal to Maximum Line-to-Ground Operating Voltage of the arrester is applied and waveforms of applied voltage and total leakage currents are recorded.
2. A voltage of 10% above Maximum Line-to-Ground Operating Voltage is applied to the same arrester and their waveforms are recorded.

3. Voltage is increased so that peak value of the resistive current is 1 mA, this value of voltage and the waveforms are recorded.
4. Finally, voltage is further increased till the peak value of the resistive current is 2 mA and this value of voltage and the waveforms are recorded.

Recorded waveforms and voltages derived from a 33 kV arrester are shown in Fig. A.1.

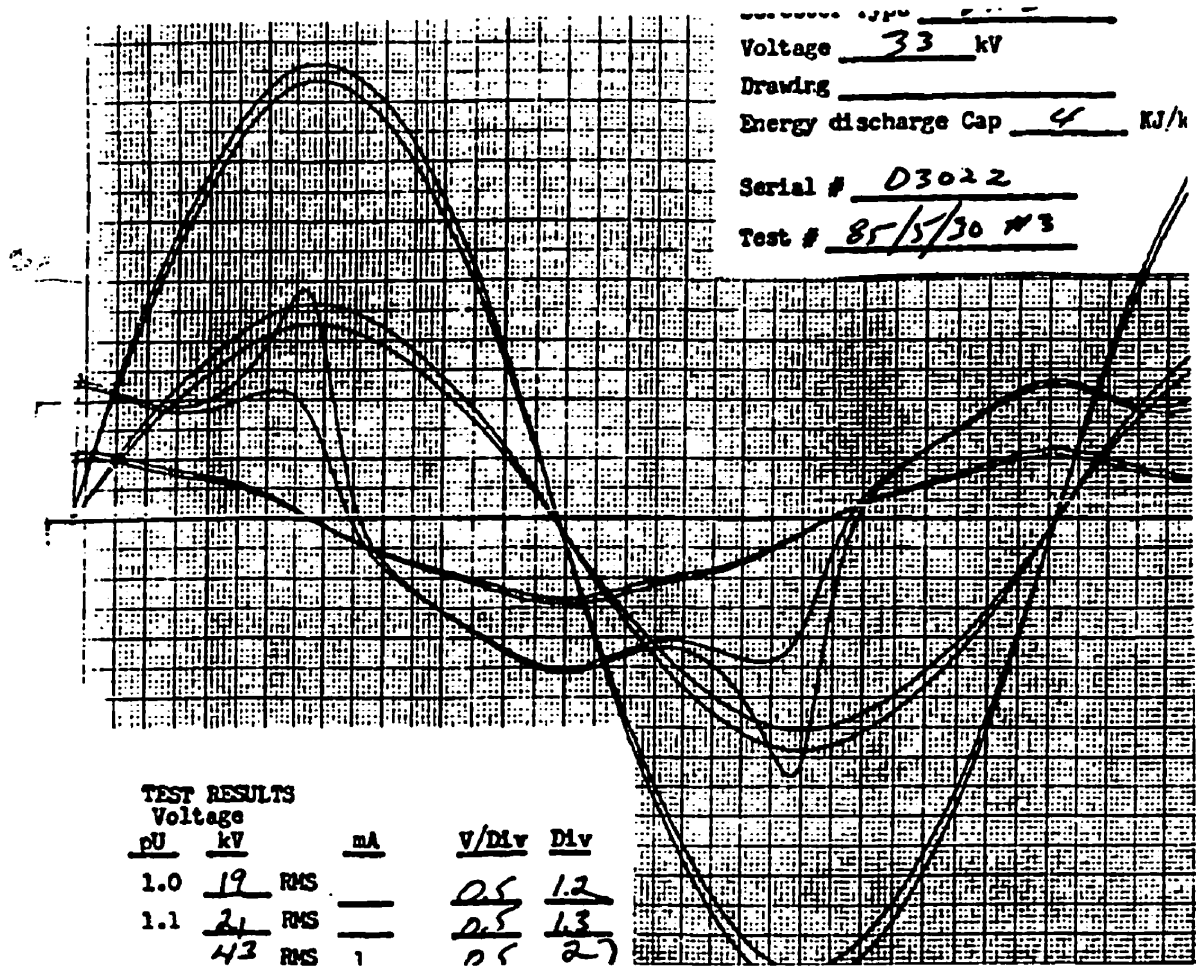


Fig. A.1 Test Data sheet for a 33 kV arrester [Courtesy Manitoba Hydro]

A.2 Voltage and Total Current Waveforms of the MOSA

Application of the Compensation Technique requires the availability of waveforms of applied voltage across the arrester and total current. Furthermore these waveforms should be in digital format which can be used by a software program written in Matlab. Unfortunately, waveforms only in paper format were available and one of these test sheets is shown in Fig. A.1. To overcome this problem, using an Image Editor, one of the voltage waveforms in Fig. A.1. and its corresponding current waveform were converted to a digital file manually. For this purpose voltage corresponding to resistive current of 1 mA was selected. The horizontal axis (time) was divided into 286 points per period. Corresponding to each point voltage and current were calculated. Fig A.2 shows the reproduction of voltage and current using data points obtained.

A.3 The $v-i_r$ Characteristic of the MOSA

The Compensation Technique can be used on the waveforms shown in Fig. A.2 to yield the effective capacitance of the 33 kV arrester used in the test. Knowing capacitance and harmonics in the voltage we can find the capacitive current. Subtraction of the capacitive current from the total current yields the resistive current. Fig. A.3 shows voltage, capacitive current and resistive current corresponds to the MOSA considered.

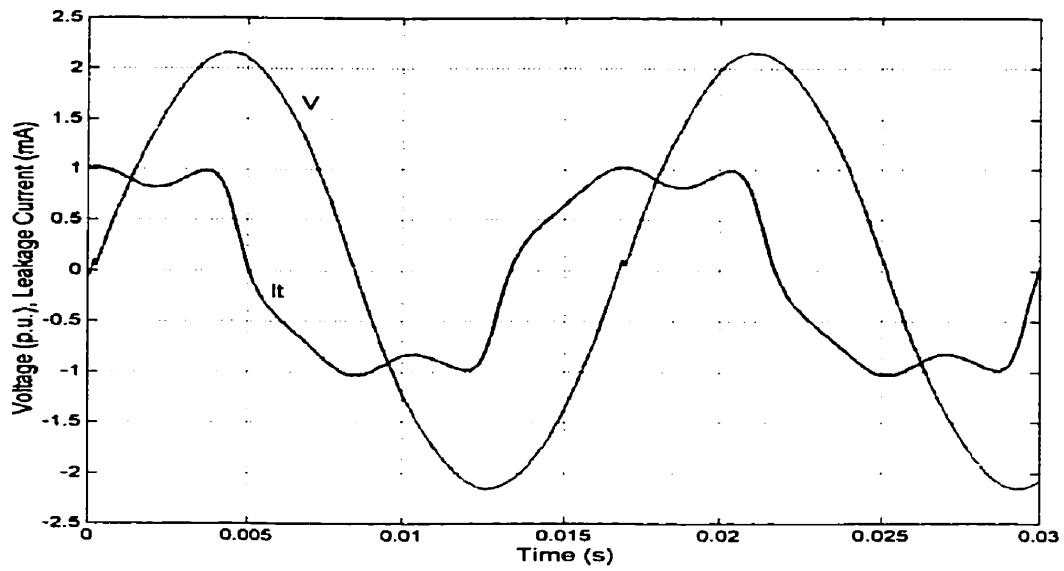


Fig. A.2 Applied voltage and total leakage current.

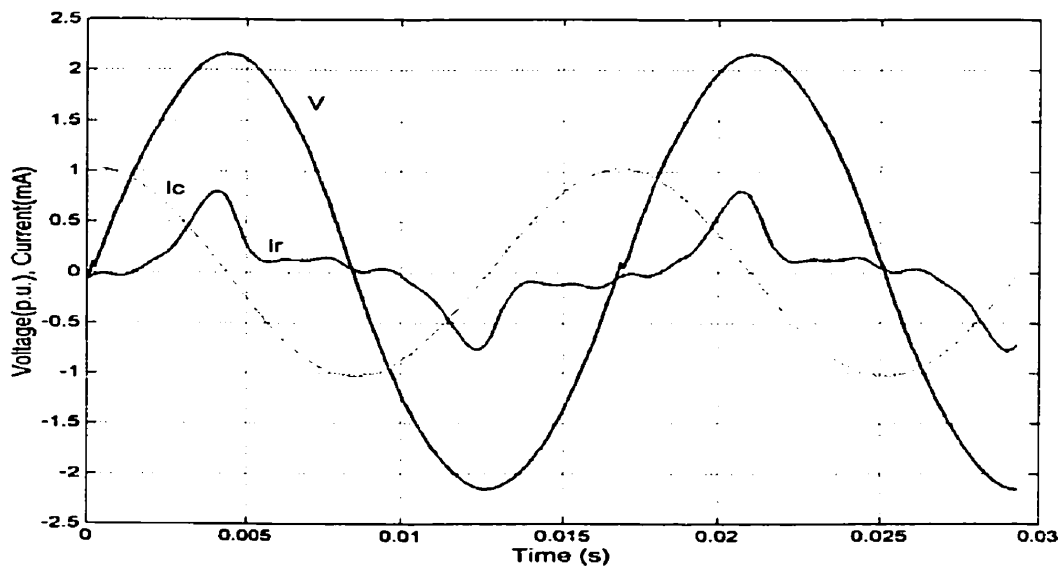


Fig. A.3 Waveform of applied voltage, capacitive current and resistive current of MOSA.

The $v-i_r$ characteristics of the MOSA is shown in Fig. A.4.

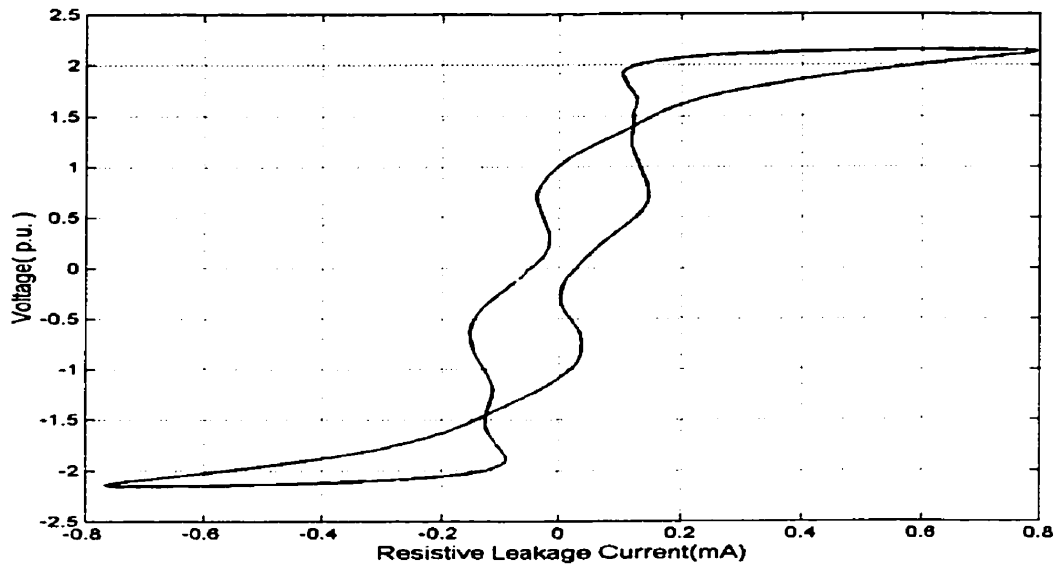


Fig. A. 4 $v-i_r$ characteristics curve of MOSA

A.4 Application of Compensation Technique to Manitoba Hydro Test Procedure

As demonstrated above, using the Compensation Technique one can find not only the applied voltage and peak resistive current, but also the $v-i_r$ characteristics. This information will complement the test procedure. It would be interesting to know how the $v-i_r$ characteristics change with ageing at elevated voltages considered in this test procedure. Further work in this area is required before arriving at a conclusion. To incorporate the Compensation Technique into Manitoba Hydro test procedure, only a digital oscilloscope, and a personal computer and Matlab are required.

Reference List

- [1] S. Shirakawa, F. Endo, H. Kitajima, S. Kobayashi, K. Kurita, "Maintenance of Surge Arresters by a Portable Arrester Leakage Current Detector", *IEEE Trans. Power Delivery*, Vol. 3, No 3, July 1988, pp.998-1003.
- [2] A. Menth, P. Streit, B. Knecht, "Present State and Development Potential of Solid State Varistors", *Proceedings of the Brown Boveri Symposium on Surges in High-Voltage Networks*, Baden, Switzerland, Sept. 3-4, 1979, pp. 283-299.
- [3] A. Schei, K.H. Weck, "Metal Oxide Surge Arrester in AC Systems Part 1: General Properties of the Metal Oxide Sure Arrester", *Electra*, N^o 128, 1989, pp. 100-105
- [4] Hanxin Zhu, "Investigation of On-site Diagnostic Testing of Metal Oxide Surge Arresters", M.Sc. thesis, University of Manitoba, April 2000.
- [5] Liu Xuezhong, Liu Fuyi, "The Influence of Varistor Disk Capacitance of MOV Arrester on Its Voltage Distribution", *The 6th International conference on Properties and Application of Dielectric Materials*, Xi'an, China, June. 21-26, 2000, pp. 761-764.
- [6] Japanese comment on IEC-TC37 WG-4 (Secretary), 3 September 1981, "Test Circuit for Measuring Resistive and Capacitive Component of Leakage Current".
- [7] Yue Chang, Jiali Qian, "Analysis on Resistive Leakage current of ZnO Surge Arresters Detected LCD-4 Instrument-Three Phase", *High Voltage Techniques (Chinese)*, Vol. 21, No. 4, 1995, pp. 35-36.
- [8] Yue Chang, Jiali Qian, "Analysis on Resistive Leakage current of ZnO Surge Arresters Detected LCD-4 Instrument-Single Phase", *High Voltage Techniques (Chinese)*, Vol. 21, No. 2, 1995, pp. 77-80
- [9] Yimei Jia, Fuheng Xu, "Method to Measure Leakage Current of ZnO Arresters On-line", *Journal of Wuhan University of Hydraulic and Electric Engineering*, 1995, pp.30-35.
- [10] C. Heinrich, V. Hinrichsen, "Diagnostics and Monitoring of Metal-Oxide Surge Arresters in High-Voltage Networks-Comparison of Existing and Newly Developed Procedures", *IEEE Trans. Power Delivery*, Vol. 16, No 1, July 2001, pp.138-143.
- [11] H. Breder, T. Collin, "Supervision of Gapless Zinc-Oxide Surge Arresters", *IEE Conference on Lightning and Power Systems*, June 1984, pp. 91-95.

-
- [12] J.Lunquist, L.Stenstrom, A.Schei, B.Hansen, "New Method for Measurement of the Resistive Leakage Current of Metal-oxide Surge Arresters in Service", IEEE Trans. Power Delivery, Vol.5, No.4, November 1990, pp.1811-1822.
- [13] V.Hinrichsen, G.Scholl, M. Schubert, T. Ostertag, "Online Monitoring of High-Voltage Metal-Oxide Surge Arresters by Wireless Passive Surface Acoustic Wave (SAW) temperature Sensor", 11th International Symposium on High Voltage Engineering, London, England, Aug., 1999.
- [14] Hanxin Zhu, M.R.Raghuveer, "Influence of Harmonics in System Voltage on Metal Oxide Surge Arrester Diagnostics", IEEE Conference on Electrical Insulation and Dielectric Phenomenon, Austin, TX, USA, Oct. 17-20, 1999, pp.542-549.
- [15] Tekronix TDS 340 instruction manual.
- [16] B. Knecht, "Solid-State Arresters", Proceedings of the Brown Boveri Symposium on Surges in High-Voltage Networks, Baden, Switzerland, Sept. 3-4, 1979, pp. 305.
- [17] G.E. Pike, "Electronic Properties of ZnO Varistors: A New Model", Proceedings of the Materials Research Society Annual Meeting. Vol 5, 1982, New York, NY, USA p 369-379
- [18] Haefly 470 user manual.
- [19] A. Haddad, H.S.B. Elayyan, D.M. German,,R.T. Waters, "ZnO Surge Arrester Elements with Mixed Direct and 50 Hz Voltages", IEE Proceedings, Part A: Science, Measurement and Technology Vol. 138, No. 5 Sep 1991 pp 265-272.
- [20] S.N. Fernando, M.R.Raghuveer, "Technique to Examine the Influence of Voltage Harmonics on the Leakage based MOSA Diagnostic Indicator", IEEE Conference on Electrical Insulation and Dielectric Phenomenon, Victoria, BC, Canada, Oct. 15-18, 2000, pp.596-599.
- [21] V.Hinrichsen, R.Peiser, "Simulation of the AC-Performance of Gapless ZnO Arrester", 5th International Symposium on High Voltage Engineering, Braunschweig, Germany, Aug. 24-28, 1987, 4 pages.
- [22] E.G. Maier, R.M. Rudolph, W. Schmidt, F. Hunziker, "Voltage Distribution and Polution Performance of Metal Oxide Arrester", International Conference on Large High Voltage Electric Systems, CIGRE Paris, Fr p 33. 12.
- [23] PSCAD user manual.
- [24] S.N. Fernando, M.R.Raghuveer, "Simulation of Metal Oxide Arrester Diagnostics Including Stray Capacitance", 12th International Symposium on High Voltage Engineering, Bangalore, India, Aug. 20-24, 2001, accepted for publication.